

Spherical Indentation of Magnetostrictive Materials

by

Thomas J. Nugent, Jr.

B.S., Physics, 1994

University of Illinois at Urbana-Champaign

Submitted to the Department of Materials Science and Engineering
in partial fulfillment of the requirements for the degree of


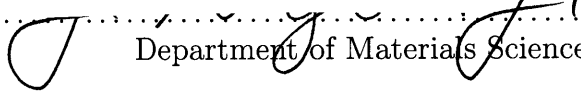
Master of Science in Materials Science and Engineering

at the

MASSACHUSETTS INSTITUTE OF TECHNOLOGY

September 1999

© Massachusetts Institute of Technology 1999. All rights reserved.

Author 
 Department of Materials Science and Engineering
August 6, 1999

Certified by
Professor Subra Suresh
R.P. Simmons Professor of Materials Science and Engineering
Thesis Supervisor

Accepted by
Professor Linn W. Hobbs
John F. Elliott Professor of Materials
Chairman, Departmental Committee on Graduate Students

Spherical Indentation of Magnetostrictive Materials

by

Thomas J. Nugent, Jr.

Submitted to the Department of Materials Science and Engineering
on August 6, 1999, in partial fulfillment of the
requirements for the degree of
Master of Science in Materials Science and Engineering

Abstract

A novel theoretical framework for analysis of indentation of magnetostrictives, based upon a linear material response model, is developed. The governing set of partial differential equations is solved for the case of an incompressible material, resulting in a solution which predicts the relationship between the change in magnetic flux and the applied load near the area of contact between the indenter and the specimen. This relationship (referred to as a Φ - P curve) and the relationship between the applied load and the indenter displacement (a P - h curve) together give a "signature" of the magnetostrictive response of a given material. Quantitatively, the flux change is predicted to be very small.

A preliminary design concept of an experimental apparatus for the instrumented indentation of magnetostrictive materials is presented. This design allows for the simultaneous measurement of load, displacement, and magnetic flux. These measurements, in conjunction with the theoretical framework, provide a new method for the characterization of magnetostrictive materials in bulk and thin-film form.

Thesis Supervisor: Professor Subra Suresh

Title: R.P. Simmons Professor of Materials Science and Engineering

Acknowledgements

If your life is free of failures, you're not taking enough risks.

—unknown

I want to first thank my advisor, Subra Suresh, for his support and encouragement throughout my tenure in the Laboratory for Experimental and Computational Micromechanics (LEXCOM). He has been an excellent advisor and supportive of all I have done. I have learned much from him through his guidance in my research and writing.

This work would not have been possible without the efforts of Antonios Giannakopoulos. His vast knowledge of mathematical mechanics helped guide our path in seeking solutions to the problems we set up. Our discussions enlightened me in many areas.

The Department of Defense National Defense Science and Engineering Graduate Fellowship program is greatly appreciated for financially supporting me with an NDSEG fellowship for the past two years.

Professor Bob O'Handley was a great help in finding material property data, and helping me understand magnetic behavior of materials. I also appreciate his lending me the use of some magnetic measurement equipment. Steve Murray helped me to design the solenoid and pickup coil, and helped me perform the VSM measurements.

I owe a great many thanks to George Labonte for all of his help. I could not have performed the experiments I did without his helping me design and set up experimental equipment. He put up with my constant requests, and showed me how to get the equipment and materials I needed as well as did much machine shop work for me.

Thanks to Krystyn Van Vliet of LEXCOM for all her indentation advice, as well as her excellent editing help. Thanks are due to Toby Freyman for his help with programming LabView. Thanks to Raj Vaidyanathan for the use of his indenter head to help calibrate my indenter system. And thanks to Andrew Gouldstone for his editing help and his humor.

Mel Goodfriend and Mike Brooks at Etrema are appreciated for their help with acquiring and polishing Terfenol-D. Thanks to M. Masteller at Carpenter Technology for donating sheets of Hiperco-27 and Hiperco-50. Scott Young and Jeff Dierker at LakeShore Cryotronics and Dave Shain of Shain Associates are appreciated for discussions of fluxmeters and fluxmeter probes, as well as the demonstration of a new fluxmeter. Thanks to Yin Lin Xie of CMSE and Raj Vaidyanathan for polishing help. Peter Morley of the MIT Central Machine Shop for his many useful design suggestions and speedy work.

I thank my parents for all that they did throughout my life that enabled me to come this far. Their faith in my abilities gave me the momentum to continually progress, and their encouragement helped

me in times of doubt.

Last but definitely not least, I thank my wife, Elizabeth, for all of her support, understanding, and helpful discussions of materials science. She helped bring this thesis to a speedy conclusion with useful editing and great programming assistance in Mathematica. Her encouragement kept me going, and her just “being there” kept me sane at times.

There is a part of me that wants to write, a part that wants to theorize, a part that wants to sculpt, a part that wants to teach.... To force myself into a single role, to decide to be just one thing in life, would kill off large parts of me.

—H. Prather

Contents

Acknowledgements	4
1 Introduction	13
1.1 Electromagnetism	14
1.2 Magnetostriction	17
1.3 Indentation	20
1.4 Description of Variables	20
1.5 Motivation	24
1.6 Outline	25
2 Problem Formulation	27
2.1 The Problem	27
2.2 Literature Review	28
2.3 Objectives	31
3 Linear Material Model	33
3.1 Assumptions	33
3.2 Equilibrium Equations	34
3.3 Other Information	35
3.4 Constitutive Equations	37
3.5 Partial Differential Equations	40
3.6 Boundary Conditions	44
3.7 Solution	46
3.8 Measureable Quantities	57
3.9 Outline of Other Solution Methods	59

4	Experimental Design	63
4.1	Material Properties	63
4.2	Apparatus	64
4.3	Experimental Procedure	74
5	Conclusions and Recommendations	77
5.1	Conclusions	77
5.2	Future Work	78
A	Classical Indentation Results	81
A.1	Geometry	81
A.2	General Values	81
A.3	Displacements and Stresses	83
B	Unit Conversions	87
	Bibliography	89

List of Figures

1-1	Magnetization curves for para-, dia-, and ferromagnetic materials.	16
1-2	Magnetostrain λ versus magnetic field H	18
1-3	Typical P - h curve; this is for unmagnetized Terfenol-D.	22
1-4	Indentation system	23
3-1	Plot of the differential function Γ vs. r/a	51
3-2	Comparison of the indentation PDE Γ_{in} to the fitting function \mathcal{F}_{in}	52
3-3	The convergence of the fitting function constants.	55
3-4	Comparison of the indentation PDE Γ_{out} to the fitting function \mathcal{F}_{out}	56
3-5	The final form of a) H_r and b) H_z	57
3-6	General functional behavior of d_{33}	62
4-1	A diagram of a basic indenter/pickup coil arrangement.	66
4-2	Close-in view of the indenter arrangement.	67
4-3	Cross-sectional view of the indenter/solenoid/iron yoke system.	68
4-4	Perfect and sheared magnetization curves, in arbitrary units.	69
4-5	Indenter head design conditions for indentation of Terfenol-D.	71
4-6	Indenter head design conditions for indentation of Hiperco-50.	72
4-7	Photo of experimental setup	73
4-8	Designs for a Hall probe magnetic indenter.	74
A-1	Coordinate system and property values for indentation	82
A-2	r displacement vs. r/a at the surface under a spherical indenter	84
A-3	z displacement vs. r/a at the surface under a spherical indenter	84
A-4	Stresses vs. r/a at the surface under a spherical indenter	85

List of Tables

1.1	Symbols used	21
3.1	Values of the constants for $r < a$	52
3.2	Values of the fitting constants for $r > a$	55
4.1	Tensor Property Values for Single Crystals	64
4.2	Miscellaneous Material Property Data	65

Chapter 1

Introduction

To see a world in a grain of sand

And a heaven in a wild flower

Hold infinity in the palm

And eternity in an hour

—William Blake

Indentation is a powerful materials characterization tool. Sharp indentation, for example, has been used to determine material hardness for a century. Hertzian theory of the elastic contact of two solids, developed in the 1880s, allowed scientists to predict the effects of indentation of a flat solid by a sphere. Only within the last 20 or so years, however, has indentation technology developed enough to allow experiments for measuring multiple material properties using Hertzian theory. Spherical indentation creates a multiaxial, three-dimensional stress state, and because that complicated stress state is well understood, indentation can be a quick and simple, yet powerful, measurement tool. In fact, indenters are now commercially available over a size scale ranging from nano-scale to macro-scale indenters; none of these, though, is suited for tests that would be appropriate for testing materials with coupled properties, such as magnetostrictive materials.

“Magnetostriction” is a second-order coupling between the mechanical and magnetic behavior of a material, first discovered by Joule in 1842 [1]. One of the most important magnetostrictive effects is the change in length of a material parallel to an applied magnetic field. Magnetostrictive materials are used in a variety of applications, including sonars [2], speakers, actuators, and transducers [1]. Understanding magnetostrictive theory is also important for applications where it is advantageous for the magnetostrictive response to be minimized, as in computer hard disks and power transformers

(i.e., applications for which it is preferred that a mechanical deformation **not** accompany a change in magnetization). About 20 years ago, so-called “giant” magnetostrictive materials were discovered, the most notable of which is Terfenol-D ($\text{Tb}_{0.3-x}\text{Dy}_{0.7+x}\text{Fe}_{2-y}$ ($0 \leq x \leq 0.03$, $0 \leq y \leq 0.1$)) [3]. These materials have a maximum magnetostrictive strain on the order of 1,000 microstrain, which is two orders of magnitude larger than traditional materials (such as Nickel).

Investigations into indentation of materials with coupled properties have only been begun recently, with the indentation of piezoelectric materials [4–6]. Taken separately, indentation and magnetostriction are research topics of great complexity and depth. The power of instrumented indentation, however, offers a new method of characterizing magnetostrictive materials. This thesis begins the investigation into indentation of magnetostrictive materials.

The remainder of this introduction first presents a brief review of relevant subjects, including electromagnetism, magnetism in materials, magnetostriction, and indentation. The symbols and variables that describe the pertinent physical quantities used in this thesis are then described. Finally, the motivation and objectives are discussed and an outline of the thesis is presented.

1.1 Electromagnetism

All electromagnetic phenomena are governed by Maxwell’s four equations. In the 1860s, James Clerk Maxwell combined disparate electromagnetic equations, correcting inconsistent parts of electromagnetic theory in the process, and put them into the form used to this day. The derivative form of these vector equations, which apply to the indenter, specimen, and the surroundings, is as follows:

$$\text{Gauss' Law} \quad \vec{\nabla} \cdot \vec{D} = \rho \quad (1.1)$$

$$\text{Maxwell–Faraday Law} \quad \vec{\nabla} \times \vec{E} = -\frac{d\vec{B}}{dt} \quad (1.2)$$

$$\text{Law of Conservation of Magnetic Flux} \quad \vec{\nabla} \cdot \vec{B} = 0 \quad (1.3)$$

$$\text{Ampère's Circuital Law} \quad \vec{\nabla} \times \vec{H} = \frac{d\vec{D}}{dt} + \vec{J}_{\text{free}} \quad (1.4)$$

(See Table 1.1 for a list defining symbols used in this thesis.) Equation 1.1 relates the divergence of the displacement field \vec{D} to an electric charge density ρ . Equation 1.2 relates the electric field \vec{E} created by a temporally variable magnetic flux density \vec{B} . Faraday’s law of electromagnetic induction, which states that

$$V = -\frac{\partial\Phi}{\partial t} \quad (1.5)$$

(where V is the electric voltage and Φ is the magnetic flux inside a given area), can be derived from the Maxwell–Faraday law. Electromagnetic induction is the mechanism used to detect a changing magnetic field with a pickup coil, as will be discussed in Ch. 4. Eq. 1.3 implies that there are no magnetic monopoles, i.e., there are no magnetic “charges” as there are electric ones. It further implies that magnetic field “lines” can not terminate at the surface of a material, as electric field lines do at the surface of a conductor. Finally, Eq. 1.4 gives the magnetic field \vec{H} produced by free electric currents \vec{J}_{free} and by temporally changing electric displacement fields.

A theory of potentials which aids in the solution of problems exists for electromagnetic theory. Electric problems can be solved solely by utilizing an electric potential ϕ such that $\vec{E} = -\nabla\phi$. One advantage of such a scalar potential ϕ is that a constant can be added to it without changing the solution for \vec{E} (and thus the point of “zero” potential can be redefined for convenience).

The analogous method of solving magnetic problems requires a vector potential \vec{A} such that $\vec{B} = \nabla \times \vec{A}$. When there are no free currents, however, a magnetic scalar potential ϕ_M may be defined that will fully satisfy Maxwell’s equations. The scalar potential is easier to use because it involves fewer variables.

Magnetic fields are created by the motion of electric charges, either as macroscopic current in a conducting wire or as the microscopic “current” produced by bound electrons (electron spin generally dominates over the electron orbital motion contribution to the total magnetic field). The magnetic flux density \vec{B} is thus the sum of a global applied magnetic field \vec{H} and the local atomic field \vec{M} (referred to as the magnetization), multiplied by the permeability of free space μ_0 :

$$\vec{B} = \mu_0(\vec{H} + \vec{M}) \quad (1.6)$$

All three terms (\vec{B} , \vec{H} , and \vec{M}) are often discussed as if independent from each other. For a perfectly magnetically linear material, however, \vec{M} is directly proportional to the applied field \vec{H} ; the proportionality constant is referred to as the susceptibility χ :

$$\vec{M} = \chi\vec{H} \quad (1.7)$$

and thus the magnetic flux relations can be written as $\vec{B} = \mu_R\vec{H}$, where $\mu_R = \mu_0(1 + \chi)$.

The interaction of the magnetic fields due to each atom in a solid creates a plethora of material behaviors. Materials may be categorized by their macroscopic responses to an applied field. Paramagnetic materials are those for which the susceptibility is small but positive, thus creating a magnetic flux density slightly larger than that due to the magnetic field itself: $\chi \approx 10^{-5}$ – 10^{-3} . Diamagnetic materials are those for which the susceptibility is small and negative, and thus the magnetic flux density is

slightly smaller than it would be otherwise: $\chi \approx -10^{-5}$. Finally, ferromagnetic materials, the materials which are of greatest relevance to this thesis, exhibit extremely large susceptibilities, up to $\chi \approx 10^6$ in modern materials. The high susceptibilities are due to the overlap of electron orbitals between atoms; the “exchange” energy due to this overlap is minimized when the magnetic moments (i.e., the electron spins) are parallel (the sum of all those parallel spins leads to the large susceptibilities of ferromagnetic materials). Magnetostriction is generally only observed in ferromagnetic materials. Soft ferromagnetic materials exhibit a linear relation between specimen magnetization and applied magnetic field, whereas the magnetization of hard magnetic materials is dependent on the magnetization history of the specimen, i.e., there is hysteresis in the magnetization. Figure 1-1 shows the magnetization response to an applied magnetic field for the above types of magnetic materials.

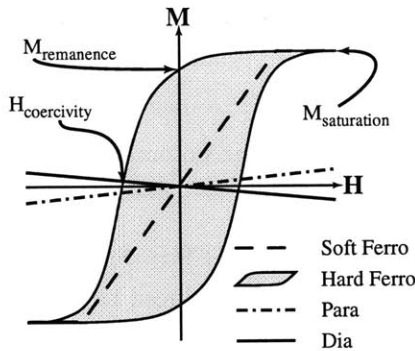


FIGURE 1-1: Magnetization curves for para-, dia-, and ferromagnetic materials.

While the exchange energy tends to align the magnetic moments with each other, there is another energy term, the anisotropy energy, which tends to align the magnetic moments with a particular crystal direction. This direction is referred to as the easy axis of magnetization. The internal energy of the system increases (as a function of angle between the easy axis and the magnetization axis) as the magnetization is rotated away from the easy axis. The general form of the anisotropy energy for cubic crystals is

$$E = K_1(\alpha_1^2\alpha_2^2 + \alpha_2^2\alpha_3^2 + \alpha_3^2\alpha_1^2) + K_2\alpha_1^2\alpha_2^2\alpha_3^2 \quad (1.8)$$

where K_1 and K_2 are the anisotropy constants (and should not be confused with the Bessel functions $K_n[x]$, which will be used later), and α_1, α_2 , and α_3 are the direction cosines with respect to the edges of the cubic unit cell. Some magnetostrictive materials, such as Hiperco-50 and Terfenol-D, have anisotropy energies that are nearly zero; among other things, this property implies that the change in magnetization is large for a given applied stress.

The magnetostatic energy of a specimen can be reduced via the formation of domains. A domain is a region of material inside which the magnetization points uniformly in the same direction. Different domains are, however, oriented in different directions. Appropriate distributions of domain orientations can result in a bulk magnetization of zero (i.e., all the domains are randomly oriented or pointing anti-parallel). Domains are generally on the order of 10 to 100 microns in diameter. A continuum mechanics approach, such as that taken in this thesis, is appropriate when the size scale of the system (in this case, the contact area) is significantly larger than the domain size.

Domain walls are the regions between domains where the local magnetization direction rotates from the orientation of one domain to the orientation of the other. The thickness of domain walls is a result of the balance between the exchange energy (which tends to align adjacent spins) and the anisotropy energy (which tends to align spins with the easy axis). Walls are characterized by the angle between the magnetization directions of the domains they separate; 180° and 90° walls are particularly common.

One final point about magnetism in materials is worth noting. A specimen magnetized along its length and with no ends (i.e., either a closed ring or an infinitely long rod) exhibits an ideal magnetization curve. Other geometries, however, are subject to an internal demagnetizing field due to the fact that the magnetic flux lines do not close back on themselves via a path that resides entirely in the specimen. The demagnetizing field “shears” the magnetization curve over (see discussion in Chapter 4), which is equivalent to reducing the susceptibility of the sample. This effect will be an important design consideration for the solenoid which will be used to magnetize our samples.

1.2 Magnetostriction

Magnetostriction¹ is a mechanical deformation or property change in a specimen due to a magnetic field, or the development of a magnetization change in response to a mechanical strain. Any ferromagnetic material (most of which are also magnetostrictive) has a spontaneous magnetization, as stated above. Magnetic domains, within which all magnetic moments point in the same direction, can be distributed with random orientations (assuming that the net magnetization of the bulk material is zero) throughout the solid. Each domain is therefore already strained to its saturation magnetostriction (this is the volume magnetostriction). The mechanical strain due to a magnetic field is referred to as the magnetostrain; the symbol λ is often used to refer to the uniaxial magnetostrain. Changing the direction of magnetization,

¹The terms “magnetostrictive,” “piezomagnetic,” and “magnetoelastic” are used interchangeably in this thesis. In fact, they do have subtly different meanings (piezomagnetism is a linear magnetomechanical effect, whereas magnetostriction is a second-order effect that is often represented with a first-order notation [7]).

however, also changes the direction of magnetostriction, and it is this change which causes bulk strains due to magnetostriction.

There are multiple models used to represent magnetostrictive properties. One model assumes a magnetically saturated material (equivalent to a single domain), and therefore deals with saturation values. The model we use for indentation of magnetostrictives is developed from a thermodynamic approach [1]. This method allows a bulk perspective, and allows for a range of magnetizations (this is possible by having multiple domains, each of which can be oriented in a different direction; summation of the domains produces the bulk magnetization). Figure 1-2 shows the uniaxial magnetostrain λ developed parallel to a uniform applied magnetic field \vec{H} .

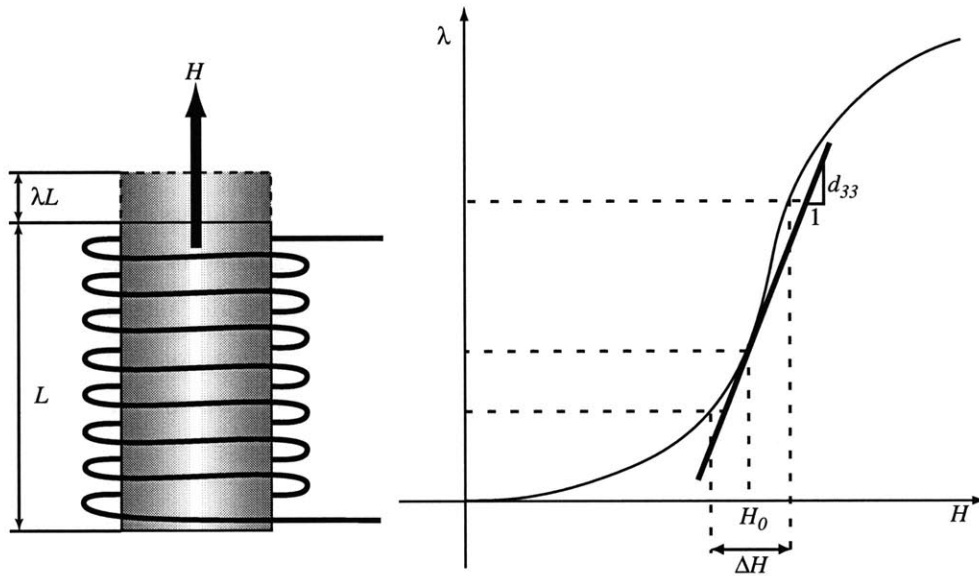


FIGURE 1-2: Magnetostrain λ versus magnetic field H

1.2.1 Types of Magnetostrictive Response

There are a few magnetoelastic effects which are particularly relevant to this work. The volume magnetostriction is, as the name implies, a uniform change in total volume with magnetization. This term also depends on temperature (and it is through balancing the temperature dependence of volume magnetostriction against the thermal expansion coefficient that, for example, the Invar Ni-Fe alloys are able to keep a constant volume over a large temperature range).

Joule magnetostriction refers to the anisotropic strain dependence of a material on an applied field. When the term “magnetostriction” is used by itself, it often refers to Joule magnetostriction. This is

because one of the primary uses of magnetostrictive materials is in actuators, in which an applied field is oscillated slightly and causes an oscillating change in the strain parallel to the field, see Figure 1-2.

The Wiedemann effect refers to torsional, instead of longitudinal, magnetostrictive response. It is usually created by running a current through a cylindrically magnetized cylinder; the resultant torsional magnetization causes a torsional strain.

The ΔE effect is the change in elastic modulus with magnetic field. An applied stress causes a change in magnetic field, which creates a magnetostrain. Therefore (especially at low applied fields) the material strains more than it otherwise would, and thus has a lower elastic modulus at low fields than it would were it not magnetostrictive. The modulus reaches a maximum at saturation magnetization.

1.2.2 Linear Magnetoelastic Model

The magnetostrictive constants defined in IEEE Standard 319 can be represented in tensor notation, but it is important to realize that it is not a true tensor property (as opposed to the elastic or piezoelectric properties, which are true tensor properties). It is written as a 3rd rank tensor because it relates a strain or stress (2nd rank) to a magnetic field or field density (1st rank).

In a manner similar to what is done for third rank piezoelectric tensors, the magnetostrictive “tensor” can be contracted from a three-subscript notation to two-subscript notation:

$$d_{ijk} = \frac{\partial B_k}{\partial \sigma_{ij}} = \frac{\partial \varepsilon_{ij}}{\partial H_k} \quad (1.9)$$

by means of contracting the strain/stress component in the same way that strain/stress tensors and stiffness/compliance tensors are contracted: 11 \rightarrow 1, 22 \rightarrow 2, 33 \rightarrow 3, 23 or 32 \rightarrow 4, 13 or 31 \rightarrow 5, and 12 or 21 \rightarrow 6. The representation then reduces to

$$d_{mn} = \frac{\partial B_m}{\partial \sigma_n} = \frac{\partial \varepsilon_n}{\partial H_m} \quad (1.10)$$

Therefore the first number refers to the magnetic field (and hence ranges from 1 to 3), and the second number refers to the stress/strain field (and can range from 1 to 6). Note that $d_{ijk} \rightarrow d_{kn}$ [1].

These magnetostrictive constants are useful in that they measure the amount of change in strain for a given change in magnetic field. Generally, only the maximum value for d_{33} (and the magnetic field strength at which it occurs) is reported in the literature, as that is the parameter most important in the design of transducers.

1.3 Indentation

Indentation has been a useful technique in materials characterization for nearly a century. Since Hertz developed the theory of indentation of two elastic solids [8], indentation has been used and studied extensively. A comprehensive introduction to the mechanics of indentation can be found in Johnson [8].

Indentation provides a very interesting example of mechanical behavior. Hertz solved the general problem of pressing two spheres into each other (see Appendix A for details) [8] which can be reduced to pressing a sphere into a flat surface by setting the radius of one sphere to infinity. Hertz's results give the stresses and displacements on the surface only. The potential methods of Boussinesq and Cerruti [8] can be used to determine the stresses and displacements throughout an entire body, but generally require numerical solution; Johnson [8] only gives the solution on the surface. Hamilton [9] presents a simpler way to determine the displacements and stresses throughout the body, and in fact gives a closed form algebraic solution for the stresses.

One of the most important results to come out of the classic indentation investigations was the prediction that related the applied normal force P to the depth of indentation h for linear elastic isotropic materials:

$$P = Ch^{\frac{3}{2}} \quad (1.11)$$

where $C = \frac{4}{3}\sqrt{RE^*}$, R is the composite radius of the two bodies, and E^* is the composite elastic modulus (see Appendix A for more details). Both load P and displacement h are relatively easy to measure experimentally. Technological advances enabled the accurate measurement of these quantities, and thus enabled the use of P - h curves as a materials characterization tool. By performing an indentation test (and assuming that the properties and the geometry of the indenter are known), then, for example, the Young's modulus of a specimen can be deduced from the C value obtained from fitting the P - h response of an indentation test.

Indentation is an important test of materials because of its well-characterized multiaxial behavior. The stress state throughout the body is known, and other related phenomena (such as pile-up or sink-down near the indenter) are well-correlated with the elastoplastic properties of the indenter and the material.

1.4 Description of Variables

Table 1.1 lists the symbols used in this thesis, their name, and their units. Note that $\mu_0 = 1.254 \cdot 10^{-6}$ H/m and $\epsilon_0 = 8.854 \cdot 10^{-12}$ F/m. (See Appendix B for a list of unit conversions.)

Symbol	Description	Units
\vec{B}, B_i, \tilde{B}	Magnetic flux density	T
\vec{M}, M_i	Magnetization	A/m
\vec{H}, H_i, \tilde{H}	Magnetic field	A/m
Φ, Φ_i	Magnetic flux	Wb
ϕ_M	Magnetic Scalar Potential	A
$\mu, \mu_{ij}, \tilde{\mu}$	Permeability	H/m
χ	Susceptibility	-
\vec{E}, E_i	Electric Field	V/m
\vec{D}, D_i	Electric Displacement	C/m ²
\vec{P}, P_i	Polarization	C/m ²
ϕ or V	Electric Scalar Potential	V
ϵ	Permittivity	F/m
\vec{J}	Current Density	A/m ²
$\sigma, \sigma_{ij}, \tilde{\sigma}$	Stress	Pa
$\epsilon, \epsilon_{ij}, \tilde{\epsilon}$	Strain	-
u, u_i	Displacement	m
a	Contact Radius	m
C_{ijkl}, \tilde{C}	Stiffness tensor	Pa
c_{ij}	Simplified stiffness tensor	Pa
C	Curvature of a P - h curve	N/m ^{1.5}
E	Young's Modulus	Pa
ν	Poisson's ratio	-
$\nu_{ij}, \tilde{\nu}$	Reluctivity	m/H
λ	Magnetostrain	-
$e_{ij}, e_{ijk}, \tilde{e}$	Magnetostriction coefficient	T
$d_{ij}, d_{ijk}, \tilde{d}$	Magnetostriction coefficient	T/Pa
γ	Normalized radial position, r/a	-
Θ	Composite Variable = $(1 - \nu^2)p_0 e_{15}/(E^* a)$	T/m

TABLE 1.1: Symbols used

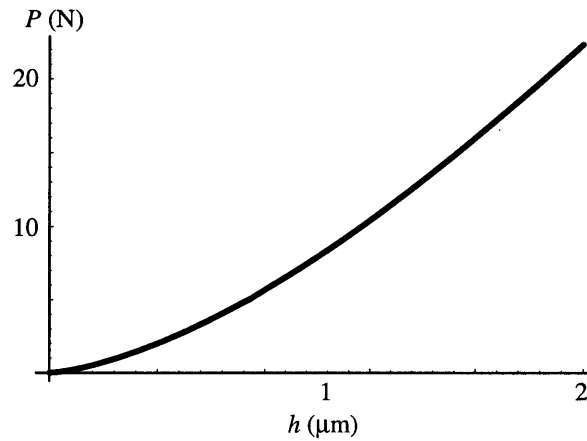


FIGURE 1-3: Typical P - h curve; this is for unmagnetized Terfenol-D.

As seen in Eq. 1.6, \vec{B} is μ_0 times the sum of \vec{H} and \vec{M} . These three terms, however, are often interchanged so that any of them is the sum (or difference) of the other two. One way of looking at this is to consider \vec{H} to be a “global” magnetic field due to large-scale applied currents, whereas \vec{M} is a “local” magnetic field due to atomic-scale currents. \vec{B} , then, is the sum of these local and global variables. Perfectly linear, magnetically soft materials have no intrinsic magnetization, but can be magnetized by an applied field. In the case of a permanent (hard) magnet with no external applied field, however, both \vec{H} and \vec{B} are needed to solve for Maxwell’s equations. In this way, Eq. 1.6 is manipulated to obtain whichever magnetic variable would be considered as primary. \vec{B} is measured in Tesla or Webers (units of flux) per square meter, whereas \vec{H} and \vec{M} are measured in terms of Amperes per meter (equivalent to the amount of current per unit length of a solenoid).

The magnetic flux Φ is often described as representing the individual “lines” of magnetic field. The density of these lines is \vec{B} and defines the strength of interaction of magnetic fields, but the flux itself is extremely important. For the purposes of this work, the flux is useful for measuring the magnetic changes near the point of contact, because the pickup coil used to detect these changes is much larger than the area of the magnetic field. The field itself is of varying flux density, and so the most useful variable to measure is the total flux, since this will signal the overall change in the magnetic field.

The stress σ_{ij} and the strain ε_{ij} describe the pressure (units of Pascals) and fractional displacements (dimensionless; often expressed as a percentage) in a solid. The stiffness coefficients C_{ijkl} (given in units of Pascals) relate the stress necessary for unit strain. In indentation, the displacements u near the indenter, measured in meters, are used to determine the local deformation. The contact radius a , also measured in meters, is an extremely important length scale in determining the size of the region

in which properties are being tested.

Figure 1-4 shows the coordinate system and certain dimensional parameters for spherical indentation. Given enough material symmetries, spherical indentation is axisymmetric and therefore a cylindrical coordinate system is used. A load P is applied to a sphere of radius R , which indents to a depth h (sometimes referred to as δ), with a contact radius a .

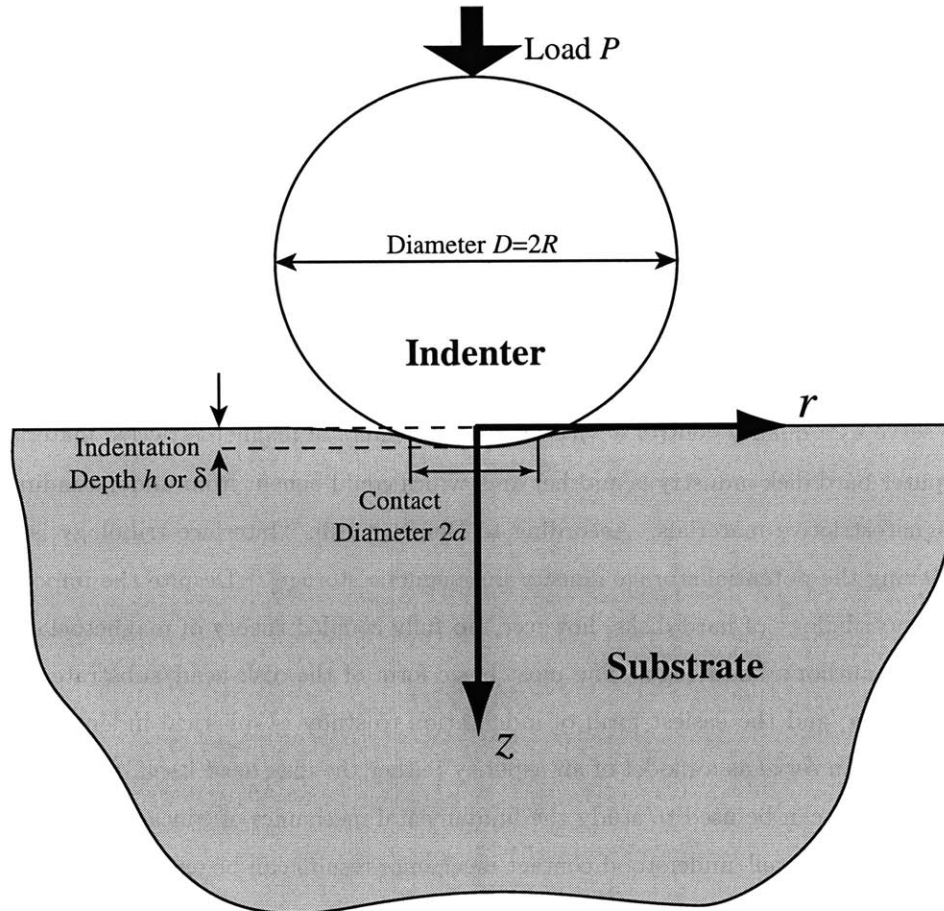


FIGURE 1-4: Indentation system

There are four magnetostriction coefficients, which relate stress or strain to magnetic field or flux density. The two most commonly discussed in this thesis are e_{ij} and d_{ij} . e_{ij} , which relates a change in stress to a change in magnetic field (or a change in flux density to a change in strain), has units of Tesla (literally, Tesla per unit strain). d_{ij} relates a change in strain to a change in magnetic field (or a change in flux density to a change in stress), and has units of meters per Amp (strain units per magnetic field units) or Tesla per Pascal. The scale of this coefficient is such that it is generally written in units of

nanometers per Amp.

1.5 Motivation

As mentioned at the beginning of this chapter, magnetostriction is important for a number of applications. Beyond this, though, magnetoelastic coupling opens a window into the study of nanotribology of an important class of magnetic materials—those used in computer hard disks.

A requirement for studying material properties and tribology is a clear understanding of the material response to stimuli. In particular, it is desirable to predict material response to a stimulus and to extract material properties from the data measured during a stimulus, i.e., the solution of both the forward and the reverse problems are desirable.

One motivation for studying the indentation of magnetostrictive materials is the need for a quick and simple yet powerful method of measuring material properties (both magnetic and elastic) of magnetostrictive materials. Such a tool would not only allow the characterization of newly developed materials; it could also serve as a quality control device for manufacturers of magnetostrictive materials.

The computer hard disk industry is another area which could benefit from understanding the indentation of magnetostrictive materials. According to Bhushan [10]: “Interface tribology is the limiting factor in achieving the potential storage density [in magnetic storage].” Despite the importance of understanding nanotribology of hard disks, however, no fully coupled theory of magnetoelastic tribology yet exists, to the author’s knowledge. The most basic form of the disk head/substrate interaction to study is indentation, and the easiest form of indentation to study is spherical indentation. In fact, a spherical indenter can serve as a model of an asperity (either the disk head itself, or a non-flat section of the substrate), and can be used to study the fundamental mechanics of contact. Using the spherical indenter as a model, the well-understood contact mechanics results can be extended, then, to the hard disk industry.

Indentation can not currently be used to study magnetostrictive materials or the tribology of magnetic materials for two reasons. First, as mentioned above, a fully coupled theory of indentation of magnetostrictive materials does not exist. Second, there is no experimental apparatus which can simultaneously measure mechanical and magnetic changes. This thesis seeks to remedy both problems. Our first objective is to create a theoretical framework for analyzing the indentation of magnetostrictive materials. Our second objective is to design and construct a quantitative indentation setup for testing the same materials. More specifically, the theory should predict the form of the P - h curves, as well as an analogous form for magnetic data: Φ - P curves. The experimental setup should be able to measure

the same data.

Indentation can also be used to measure the decay of magnetization over time of a material at elevated temperatures. The magnitude of the spontaneous magnetization decreases with temperature until, above the Curie temperature, magnets lose all spontaneous magnetization. Furthermore, there is a time-dependent decay of magnetization at elevated temperatures (below the Curie temperature) for some magnets. The activation energy for depolarization was successfully measured for piezoelectrics via indentation [6], and similar capabilities are expected for indentation of magnetostrictive materials.

1.6 Outline

In Chapter 2, the formulation of the problem is presented, the relevant literature is reviewed, and the objectives of the research are outlined. Chapter 3 is the main theoretical chapter, wherein we examine the constitutive equations, apply the equilibrium conditions to them, solve the resulting partial differential equations and arrive at a general solution for a limiting case. A description of the experiments to validate this theory is included in Chapter 4. Chapter 5 summarizes conclusions and recommendations for future work. Appendix A summarizes the classical results for indentation of an elastic solid by a sphere.

Chapter 2

Problem Formulation

2.1 The Problem

Fundamentally, the challenge we face is to create a reliable and simple test which allows the determination of the magnetoelastic, as well as the elastic and magnetic, properties of a given material. “Simple” means of such a design as to be easily usable, for example, as a quality control device for a manufacturer of magnetostrictive materials. The development of such a test includes theoretical analysis as well as experimental verification.

The theoretical problem is to determine the mechanical and magnetic response of a magnetostrictive material to indentation. Indentation creates a three-dimensional state of stress, and is therefore much more complicated than the uniaxial state of stress which has generally been treated in the literature (with a few exceptions noted below). This stress state provides the benefit that it will, at least in theory, allow the simultaneous measurement of multiple material properties in a single experiment, instead of requiring multiple experiments (which would normally require different sample geometries) to accomplish the same goal. But as will be seen in Chapter 3, it is also a hindrance in that it significantly increases the difficulty of analysis. The related experimental problem is to design and test a system which has the ease-of-use of indentation, while being able to accurately measure small changes in magnetic fields.

Before analyzing the full magnetoelastic problem, it is informative to study the case of an uncoupled material, i.e., one in which the magnetic and mechanical responses are completely independent. The

uncoupled problem has a material response described by

$$\begin{pmatrix} \tilde{\sigma} \\ \tilde{B} \end{pmatrix} = \begin{pmatrix} \tilde{C} & \tilde{0} \\ \tilde{0} & \tilde{\mu} \end{pmatrix} \begin{pmatrix} \tilde{\varepsilon} \\ \tilde{H} \end{pmatrix} \quad (2.1)$$

where the variables in each matrix are themselves material property matrices: $\tilde{\sigma}$ is the stress matrix, \tilde{B} is the magnetic flux density matrix, \tilde{C} is the elastic stiffness tensor, $\tilde{\mu}$ is the magnetic permeability tensor, $\tilde{\varepsilon}$ is the strain matrix, and \tilde{H} is the magnetic field matrix. For an “uncoupled” problem, the off-diagonal terms above are zero, and hence the mechanical ($\tilde{\sigma} = \tilde{C}\tilde{\varepsilon}$) and magnetic ($\tilde{B} = \tilde{\mu}\tilde{H}$) solutions can be derived independently. A coupled, linear material, has a material response as follows:

$$\begin{pmatrix} \tilde{\sigma} \\ \tilde{B} \end{pmatrix} = \begin{pmatrix} \tilde{C} & \tilde{d}^T \\ \tilde{d} & \tilde{\mu} \end{pmatrix} \begin{pmatrix} \tilde{\varepsilon} \\ \tilde{H} \end{pmatrix} \quad (2.2)$$

where \tilde{d} is the magnetostrictive constant matrix. The mechanical and magnetic components of a coupled problem must be solved simultaneously.

Classical indentation theory gives a relation between applied load and relative displacement of the indenter to the material, also known as the P - h curve. We expect the P - h curve of a magnetostrictive material to deviate from the classical theory in predictable ways. There are more material parameters for a magnetostrictive material than a simple elastic material, however, and so an additional set of data would be needed to fully characterize the material. Prior work on indentation of piezoelectrics measured electric current as a function of time during indentation to provide such additional data [4–6].

2.2 Literature Review

Almost all of the work to date on magnetostrictive materials has been on the uniaxial case, considering only a one-dimensional stress-strain state, as well as only a one-dimensional magnetic field (i.e., considered the strain parallel to the applied field or the change in the magnetization curve for a certain stress applied in the same direction). In addition, most of the work has focused on the magnetostrain response to an applied magnetic field, with very little investigation of the effect of applied strain on the magnetic field¹. Thermodynamics dictates that these two cases are the converse of each other, and so studying one case should reveal similar information about the other case. However, we were not able to find any studies with experimental proof of this conjecture.

¹This is likely due to the fact that applications derived so far primarily rely on the magnetostrain response to an applied field.

De Lacheisserie [1] reviews the bulk of magnetoelastic research up to about 1990. All of the physical effects which fall under the term “magnetostriction” are described in [1], both experimentally and theoretically. He presents the linear magnetoelastic constitutive model used in this thesis. Material property data on a number of magnetostrictive materials are collected therein (some of which is repeated later in this work). Various applications of magnetostriction are also described.

Brown [11] provides a comprehensive review of magnetoelastic theory, much of it derived from fundamentals. He goes in depth into a full theory which includes body couples and their effects, much of which is not relevant to the present problem.

IEEE Standard 319 [7] defines the nomenclature of magnetostrictive behavior. Namely, it defines the magnetostrictive constant matrices d_{ij} , e_{ij} , h_{ij} , and g_{ij} and presents their units. All four constants are referred to simply as the “effective piezomagnetic coefficient.” It also presents the equations of state and notes which constant coefficients are non-zero. Note that, although Std. 319 describes the magnetoelastic property constants with a 3rd rank pseudotensor, it does not impose restrictions on the tensor elements due to crystal or other material symmetries.

d_{33} refers to the strain in the 3 direction due to a magnetic field applied in the 3 direction. Figure 1-2 shows the magnetostriction constant d_{33} in a graphical manner. It should be noted, however, that the d_{ij} denote not only the strain response to an applied field, but conversely the field density response to an applied stress:

$$d_{ij} = \frac{\partial \varepsilon_j}{\partial H_i} = \frac{\partial B_i}{\partial \sigma_j} \quad (2.3)$$

While d_{33} , for example, could be estimated from the slope of a strain vs. field graph, such a practice would be tedious and not extremely accurate. Unfortunately, we were not able to find any studies which presented d_{33} as a function of field (or stress). At best, the maximum value for d_{33} (d_{33}^{\max}) alone is presented. Furthermore, as mentioned above, we were not able to find any studies which demonstrated experimentally the equivalence shown in Eq. 2.3. Given the multiple mechanisms by which the magnetization state of a body can change, it would not be surprising to find that, at a given initial applied field, one mechanism is dominant under a change in the magnetic field but that a different mechanism is dominant under a change in stress. For example, at low magnetic field a change in field may cause the motion of 180° walls (which do not create any magnetostrain) whereas at the same field a change in stress might cause 90° wall motion.

Data on d_{33}^{\max} for candidate test materials such as iron and Terfenol-D are common in the literature; some of these references are listed in Section 4.1 along with the relevant values. Data for d_{15} (or e_{15} or any of the related constants), however, was much more difficult to find. Studies of the Wiedemann

effect would be expected to report this value, but the studies found instead generally reported magnetic field strengths and applied currents (which, in a magnetized cylinder, produce the mechanical torsion). One paper, by Zhakov et al [12], does provide some data on Permendur (very close compositionally to the Hiperco-50 material listed in Chapter 4), in the form of a different magnetostrictive constant h_{15} (recall that h_{ij} are magnetostrictive constants similar to d_{ij}).

Carman and Mitrovic [13, 14] derived a nonlinear constitutive model for magnetostriction which includes mechanical, magnetic, and temperature effects. The most notable part of their work is that, instead of using the standard linear magnetomechanical coupling, they use an even-powered dependence of the magnetostrain on magnetization which is, in fact, much more appropriate to the magnetoelastic coupling (because the magnetostrain is an even function of magnetization). The advantage of their theory is that only a single set of material property constants would be needed to completely characterize a material (as opposed to the linear theory, where the material “constants” are in fact highly varying functions of magnetic field and mechanical strain).

2.2.1 Indentation of Piezoelectric Materials

Results from the indentation of piezoelectric materials are useful to study because the linear constitutive models are nearly identical in form, and there are a number of similarities between the equilibrium equations which govern their behavior. The results of the research on indentation of piezoelectric materials can serve as a guide for research into indentation of magnetostrictive materials.

Giannakopoulos and Suresh [4] first solved the problem of indentation of piezoelectric materials. Starting with basic constitutive relations for coupled electromechanical systems, they derived solutions for the general case of in-plane symmetry, for both conducting and insulating indenters.

The piezoelectric results can not simply be rewritten for magnetic systems, for a number of reasons. First, the non-existence of magnetic monopoles means that the magnetic field can not be restricted at the boundary in the same manner as the electric field (where the electric potential can be set to zero by coating the surface with a conductive film and grounding that surface). Therefore the magnetostriction boundary conditions are “weaker.” Second, the piezoelectric effect is a first order (linear) effect, whereas magnetostriction is a second order effect. Finally, electric polarization is accomplished by the separation, at an atomic scale, of charges; a material is depolarized when the charges are no longer separated. A magnetostrictive ferromagnetic material, on the other hand, is always magnetized and thereby strained to its saturation magnetostrain (on a local level — on a bulk scale, it can appear to be demagnetized). Therefore, for both macroscopic as well as microscopic reasons, the indentation responses of piezoelectrics and magnetostrictives are not directly comparable.

Despite the above-mentioned differences between piezoelectric and magnetostrictive materials, there is much useful knowledge to be gained from the prior work on indentation of piezoelectrics before proceeding with magnetostrictives. Theoretically, the constitutive models for a linear response are effectively identical. Experimentally (see below), the results provide a guide as to the type of the effects (beyond direct measurement of property constants) to be examined.

Experimental work was carried out by Ramamurty *et al.* [5] and Sridhar *et al.* [6]. They demonstrated the usefulness of the indentation technique for measuring not only the mechanical, dielectric and piezoelectric properties, but also easily determining the polarization direction and measuring the activation energy for polarization decay.

Ramamurty *et al.* [5] confirmed the theory of Giannakopoulos and Suresh by showing that the curvature of the P - h curves (the C in $P = Ch^{3/2}$) depended on whether or not the material was poled as well as the electrical state of the indenter.

Sridhar *et al.* [6] determined that the poling direction could be determined simply through the sign of the quasi-current produced by indentation. They also showed that the activation energy for decay of polarization could be determined by a series of indentation tests. Finally, it was demonstrated that measurement of electric current during indentation was able to determine the direction of polarization of the specimen.

2.3 Objectives

This thesis is a first attempt at a theoretical and experimental investigation into the indentation of magnetostrictive materials. The following results are presented in this thesis:

- A basic theoretical framework for spherical indentation of magnetostrictive materials.
- A relation between magnetic flux and indenter depth (or load) for the case of an incompressible material ($\nu = 0.5$), solved using the above framework. This result can serve as a guideline for developing experimental predictions as well as for more general analytical solutions.
- The outline of a method for dealing with variation with field (or stress) in magnetostrictive property “constants”.
- The preliminary design and construction of a new instrumented indentation setup which can simultaneously measure load, depth, and magnetic flux.

Chapter 3

Linear Material Model

The Book of Nature is written in mathematical characters.

—Galileo

This chapter first covers the equilibrium and constitutive equations as well as the boundary conditions governing this system. These are combined into the general partial differential equations that need to be solved. The general solution to these equations is then outlined, and some specific cases are solved.

3.1 Assumptions

Plastic deformation strongly affects the magnetic properties of the material, and therefore all indentation experiments will be restricted to the elastic regime. (In order to accomplish this, the yield strength of the material has to be taken into consideration when designing the indenter size and maximum load.) As the model discussed in this chapter is a linear model, complete reversibility of strains and magnetizations is assumed. This also means that the system is assumed to be linear on a local scale.

The constitutive models are assumed to be fully applicable to changes in field values as well as absolute values. Thus, $\Delta\vec{B} = \mu_0(\Delta\vec{H} + \Delta\vec{M})$ is true, with respect to an initial state $\vec{B}_0 = \mu_0(\vec{H}_0 + \vec{M}_0)$. Thus the current state of the system can be ignored, and only changes in the state of the system need be studied.

3.2 Equilibrium Equations

We are assuming regular equilibrium conditions. Beginning with mechanical equilibrium, the first condition is that the sum of all forces on the body is zero (i.e., no net acceleration of the body):

$$\frac{\partial \sigma_{ij}}{\partial x_j} = 0 \quad (3.1)$$

The next condition is the small strain equations (because of the assumption of linear elasticity):

$$\varepsilon_{ij} = \frac{1}{2} \left(\frac{\partial u_i}{\partial x_j} + \frac{\partial u_j}{\partial x_i} \right) \quad (3.2)$$

The small strain equations assume continuity of displacements, and so the compatibility equations

$$\frac{\partial^2 \varepsilon_{ij}}{\partial x_i^2} - 2 \frac{\partial^2 \varepsilon_{ij}}{\partial x_i \partial x_j} + \frac{\partial^2 \varepsilon_{jj}}{\partial x_j^2} = 0$$

are redundant if the problem is formulated in terms of displacements.

The magnetic equilibrium equations were shown in Section 1.1. The first magnetic equilibrium condition sets the divergence of the magnetic flux density to zero, or alternatively states that there are no magnetic monopoles:

$$\nabla \cdot \vec{B} = 0 \quad (3.3)$$

The other magnetic equilibrium equation relates the curl of the magnetic field to the free currents and a time change in the electric displacement field (and is also called the generalized Ampère circuital law):

$$\nabla \times \vec{H} = \vec{J}_{free} + \frac{\partial \vec{D}}{\partial t} = \vec{J}_{free} \quad (3.4)$$

because we assume that $\frac{\partial \vec{D}}{\partial t}$ is zero.

3.2.1 Cylindrical Coordinates

The axisymmetry of spherical indentation together with the material symmetry allows the problem to be recast in cylindrical (r, θ, z) coordinates (see Figure 1-4). The mechanical equilibrium equations in cylindrical coordinates are

$$\frac{\partial \sigma_{rr}}{\partial r} + \frac{\partial \sigma_{rz}}{\partial z} + \frac{\sigma_{rr} - \sigma_{\theta\theta}}{r} = 0 \quad (3.5)$$

$$\frac{\partial \sigma_{rz}}{\partial r} + \frac{\partial \sigma_{zz}}{\partial z} + \frac{\sigma_{rz}}{r} = 0 \quad (3.6)$$

where r is the radial displacement away from the line of axisymmetry, z is the depth into the specimen,

and the σ_{ij} are the stress components. The small strain equations in cylindrical coordinates are

$$\varepsilon_{rr} = \frac{\partial u_r}{\partial r} \quad (3.7)$$

$$\varepsilon_{\theta\theta} = \frac{u_r}{r} \quad (3.8)$$

$$\varepsilon_{zz} = \frac{\partial u_z}{\partial z} \quad (3.9)$$

$$\gamma_{rz} = \varepsilon_{rz} = \frac{\partial u_r}{\partial z} + \frac{\partial u_z}{\partial r} \quad (3.10)$$

where u_r is the displacement in the r direction, u_z is the displacement in the z direction, and the ε_{ij} are the strain components. The divergence of \vec{B} (conservation of magnetic flux) becomes

$$\frac{\partial B_r}{\partial r} + \frac{B_r}{r} + \frac{\partial B_z}{\partial z} = 0 \quad (3.11)$$

where B_i are the components of the magnetic flux density. Ampère's law, $\nabla \times \vec{H} = \vec{J}_{\text{free}}$, becomes

$$\frac{1}{r} \frac{\partial H_z}{\partial \theta} - \frac{\partial H_\theta}{\partial z} = J_r \quad (3.12)$$

$$\frac{\partial H_r}{\partial z} - \frac{\partial H_z}{\partial r} = J_\theta \quad (3.13)$$

$$\frac{\partial H_\theta}{\partial r} + \frac{H_\theta}{r} - \frac{1}{r} \frac{\partial H_r}{\partial r} = J_z \quad (3.14)$$

where H_i are the components of the magnetic field, and the J_i are the components of the current density.

3.3 Other Information

3.3.1 Material Constants

The number of material constants influences the complexity of the problem. Property constants for the general axisymmetric case (e.g., a polycrystalline or isotropic material with a cylindrical symmetry due to an applied field) are presented in Table 4.1, and include 10 constants. But in fact, as will be shown later, the materials we chose to examine first are not very anisotropic, and we can approximate them as isotropic. This reduces the number of material constants, and simplifies considerably the involved partial differential equations.

3.3.1.1 Related Magnetostrictive Constants

Here is a brief proof that $e_{31} = -e_{33}/2$. From Chikazumi [15], the change in length of a sample along a certain direction is

$$\frac{\delta l}{l} = \frac{-B_1}{c_{11} - c_{12}} \left(\alpha_1^2 \beta_1^2 + \alpha_2^2 \beta_2^2 + \alpha_3^2 \beta_3^2 - \frac{1}{3} \right) - \frac{B_2}{c_{44}} (\alpha_1 \alpha_2 \beta_1 \beta_2 + \alpha_2 \alpha_3 \beta_2 \beta_3 + \alpha_3 \alpha_1 \beta_3 \beta_1) \quad (3.15)$$

where the α_i are domain magnetization direction cosines and the β_i denote the strain measurement direction. Then for $\alpha_1 = \beta_1 = 1$, all others set to 0, the strain parallel to the applied field (which is proportional to d_{33} and e_{33}) is

$$\left. \frac{\delta l}{l} \right|_{\parallel} = \frac{-2}{3} \frac{B_1}{c_{11} - c_{12}} \sim d_{33} \sim e_{33} \quad (3.16)$$

and for $\alpha_1 = \beta_2 = 1$, all others being 0, the strain perpendicular to the field (which is proportional to d_{31} and e_{31}) is

$$\left. \frac{\delta l}{l} \right|_{\perp} = \frac{+1}{3} \frac{B_1}{c_{11} - c_{12}} \sim d_{31} \sim e_{31} \quad (3.17)$$

Taking their ratio shows that $e_{31} = -e_{33}/2$. This reduces the number of independent magnetostrictive constants from 3 to 2.

3.3.2 Scalar Magnetic Potential

According to Jackson [16] and Popovic [17], if $\vec{J}_{\text{free}} = 0$ in the region of interest, then $\vec{\nabla} \times \vec{H} = 0$ allows the use of the magnetic scalar potential $\vec{B} = -\mu_0 \nabla \phi_M$, for the same reason that $\vec{\nabla} \times \vec{E} = 0$ allows $\vec{E} = -\nabla \phi$ (see Section 1.1). Physically, the magnetic scalar potential is directly analogous to the electric scalar potential V . As we shall see later, it may be necessary to use this scalar potential because it reduces the number of variables by one, from B_r and B_z to ϕ_M . Note that B_θ is not included because it is zero.

3.3.2.1 Notes on components of \vec{B}

The indenter/substrate system used here is, as noted in Section 3.2.1, axisymmetric. This means that $B_\theta = \frac{\partial \phi_M}{\partial \theta} = 0$ and therefore the magnetic field is irrotational about the z axis. Since $\frac{\partial \phi_M}{\partial \theta} = 0$, we can say that (since $\vec{H} = -\nabla \phi_M$)

$$B_r = -\mu_0 \frac{\partial \phi_M}{\partial r} \quad (3.18)$$

and

$$B_z = -\mu_0 \frac{\partial \phi_M}{\partial z} \quad (3.19)$$

3.4 Constitutive Equations

As discussed in Section 3.1, only changes in field values instead of absolute values will be considered. The full form of the constitutive equations below would be written in the following form:

$$\delta\bar{\sigma} = \bar{c} \delta\bar{\varepsilon} - \bar{e} \delta\bar{H} \quad (3.20)$$

$$\delta\bar{B} = \bar{e} \delta\bar{\varepsilon} + \bar{\mu} \delta\bar{H} \quad (3.21)$$

To simplify notation, however, the “small variation” δ symbol will be dropped hereafter¹.

3.4.1 General Forms

The four possible variables to use in the constitutive equations are B , H , σ , and ε . There are four possible representations. That is, there are four ways to write the linear constitutive relations, depending on which two variables we choose to be the “dependent” ones:

1. **Stress and magnetic flux density (σ , B)**

$$\begin{aligned} \bar{\sigma} &= \bar{C}^H \bar{\varepsilon} - \bar{e} \bar{H} \\ \bar{B} &= \bar{e} \bar{\varepsilon} + \bar{\mu} \bar{H} \end{aligned} \quad (3.22)$$

where \bar{C}^H are the elastic stiffness coefficients at constant \bar{H} , \bar{e} are the magnetostrictive constants, and $\bar{\mu}$ are the permeability constants.

2. **Stress and magnetic field (σ , H)**

$$\begin{aligned} \bar{\sigma} &= \bar{C}^B \bar{\varepsilon} - \bar{h} \bar{B} \\ \bar{H} &= -\bar{h} \bar{\varepsilon} + \bar{\nu} \bar{B} \end{aligned} \quad (3.23)$$

where \bar{C}^B are the elastic stiffness coefficients at constant \bar{B} , \bar{h} are the magnetostrictive constants relating the change in magnetic field to the strain, and $\bar{\nu}$ are the reluctivity (effectively the inverse of the permeability), relating the change in magnetic field to the change in magnetic field density.

3. **Strain and magnetic flux density (ε , B)**

$$\begin{aligned} \bar{\varepsilon} &= \bar{S} \bar{\sigma} + \bar{d} \bar{H} \\ \bar{B} &= \bar{d} \bar{\sigma} + \bar{\mu} \bar{H} \end{aligned} \quad (3.24)$$

¹The elastic constants do not change with stress noticeably below the yield strength, whereas the magnetostrictive constants do depend on the magnetic field. Since we assume a monotonic behavior of our materials (and the materials' magnetization curves exhibit no hysteresis; see Chapter 4), the effects of a large (rather than infinitesimal) change in an independent variable would be dealt with by integrating the constitutive equation over the proper range; see Section 3.9.3 for details.

4. Strain and magnetic field (ε, H)

$$\begin{aligned}\tilde{\varepsilon} &= \tilde{S}\tilde{\sigma} + \tilde{g}\tilde{B} \\ \tilde{B} &= -\tilde{g}\tilde{\sigma} + \tilde{\nu}\tilde{B}\end{aligned}\tag{3.25}$$

Given the mechanical equilibrium equations (which give σ as a function of ε) and the fact that experimentally, displacements u_i are measured instead of strains, it makes sense to use either the first or second form above (i.e., (σ, B) or (σ, H) representation). Therefore, the third or fourth representations will not be discussed further. It is less clear whether the (σ, B) or the (σ, H) representation is most advantageous to use. It depends on whether we follow a straight analogy from the piezoelectric case (i.e., just substitute the magnetic divergence equation for the electric one, and similarly for the curl equation) or follow a more quasistatically “symmetrical” analogy (i.e., substitute $\nabla \times \vec{H} = \vec{J}_{\text{free}}$ for $\nabla \cdot \vec{D} = \rho$ and $\nabla \cdot \vec{B} = 0$ for $\nabla \times \vec{E} = 0$.)

3.4.2 Stress and Magnetic Flux Density (σ, B) Representation

Assuming in-plane (i.e., r - θ plane) symmetry, there are only 10 independent material constants: 5 elastic, 3 piezomagnetic, and 2 magnetic. In cylindrical coordinates, the mechanical equations are

$$\sigma_{rr} = c_{11}\varepsilon_{rr} + c_{12}\varepsilon_{\theta\theta} + c_{13}\varepsilon_{zz} - e_{31}H_z\tag{3.26}$$

$$\sigma_{\theta\theta} = c_{12}\varepsilon_{rr} + c_{11}\varepsilon_{\theta\theta} + c_{13}\varepsilon_{zz} - e_{31}H_z\tag{3.27}$$

$$\sigma_{zz} = c_{13}(\varepsilon_{rr} + \varepsilon_{\theta\theta}) + c_{33}\varepsilon_{zz} - e_{33}H_z\tag{3.28}$$

$$\sigma_{rz} = c_{44}\varepsilon_{rz} - e_{15}H_r\tag{3.29}$$

and the magnetic equations are

$$B_r = e_{15}\varepsilon_{rz} + \mu_{11}H_r\tag{3.30}$$

$$B_z = e_{31}(\varepsilon_{rr} + \varepsilon_{\theta\theta}) + e_{33}\varepsilon_{zz} + \mu_{33}H_z\tag{3.31}$$

3.4.2.1 Particular Case: Isotropic Material

If we further assume that the material is isotropic (an elastically isotropic material is one for which $\frac{1}{2}(c_{11} - c_{12}) = c_{44}$), then the number of material constants reduces to 5: 2 elastic, 2 piezomagnetic (because $e_{31} = -e_{33}/2$; see Section 3.3.1.1), and 1 magnetic. For the isotropic case, $c_{13} \rightarrow c_{12}$, $c_{33} \rightarrow c_{11}$, $d_{14} = -d_{25} = 0$ and $\mu_{33} \rightarrow \mu_{11}$.²

²de Lacheisserie [8] states that in fact d_{14} has never been observed in any material.

The constitutive equations become

$$\sigma_{rr} = c_{11}\varepsilon_{rr} + c_{12}(\varepsilon_{\theta\theta} + \varepsilon_{zz}) - e_{31}H_z \quad (3.32)$$

$$\sigma_{\theta\theta} = c_{11}\varepsilon_{\theta\theta} + c_{12}(\varepsilon_{rr} + \varepsilon_{zz}) - e_{31}H_z \quad (3.33)$$

$$\sigma_{zz} = c_{11}\varepsilon_{zz} + c_{12}(\varepsilon_{rr} + \varepsilon_{\theta\theta}) - e_{33}H_z \quad (3.34)$$

$$\sigma_{rz} = c_{44}\varepsilon_{rz} - e_{15}H_r \quad (3.35)$$

$$B_r = e_{15}\varepsilon_{rz} + \mu_{11}H_r \quad (3.36)$$

$$B_z = e_{31}(\varepsilon_{rr} + \varepsilon_{\theta\theta}) + e_{33}\varepsilon_{zz} + \mu_{11}H_z \quad (3.37)$$

Later on the equations will be rewritten using the more common Young's modulus E , shear modulus G , and Poisson ratio ν . The stiffness constants are

$$c_{11} = \frac{E(1-\nu)}{(1+\nu)(1-2\nu)}, \quad c_{12} = \frac{E\nu}{(1+\nu)(1-2\nu)}, \quad c_{44} = G = \frac{E}{2(1+\nu)} \quad (3.38)$$

3.4.3 Stress and Magnetic Field (σ , H) Representation

In a similar manner, we begin with Eqs. 3.23 from Section 3.4.1, where h_{ij} are the magnetoelastic constants (analogous to e_{ij} or d_{ij}) relating strain and magnetic field. ν_{ij} is referred to as the reluctivity, and is effectively the inverse of the permeability μ_{kl} . The relationship between h_{ij} , e_{ij} , and other constants is:

$$h_{mi} = \nu_{nm}e_{ni} = \nu_{nm}d_{nk}c_{ki} \quad (3.39)$$

$$e_{mi} = d_{mj}c_{ji}^H = \mu_{nm}^\varepsilon h_{ni} \quad (3.40)$$

and from this we can see that h_{33} , h_{31} , and h_{15} are the "equivalents" to e_{33} , e_{31} , and e_{15} . (As an example: $h_{33} = \nu_{n3}e_{n3} = \nu_{33}e_{33}$ because $e_{13} = e_{23} = 0$ due to the axisymmetry of the applied magnetic field (only the H_3 component is assumed to be non-zero [1]).)

$$\sigma_{rr} = c_{11}\varepsilon_{rr} + c_{12}\varepsilon_{\theta\theta} + c_{13}\varepsilon_{zz} - h_{31}B_z \quad (3.41)$$

$$\sigma_{\theta\theta} = c_{12}\varepsilon_{rr} + c_{11}\varepsilon_{\theta\theta} + c_{13}\varepsilon_{zz} - h_{31}B_z \quad (3.42)$$

$$\sigma_{zz} = c_{13}(\varepsilon_{rr} + \varepsilon_{\theta\theta}) + c_{33}\varepsilon_{zz} - h_{33}B_z \quad (3.43)$$

$$\sigma_{rz} = c_{44}\varepsilon_{rz} - h_{15}B_r \quad (3.44)$$

$$H_r = -h_{15}\varepsilon_{rz} + \nu_{11}B_r \quad (3.45)$$

$$H_z = -h_{31}(\varepsilon_{rr} + \varepsilon_{\theta\theta}) - h_{33}\varepsilon_{zz} + \nu_{33}B_z \quad (3.46)$$

3.4.3.1 Particular Case: Isotropic Material

Applying the same simplifications as in Section 3.4.2.1

$$\sigma_{rr} = c_{11}\varepsilon_{rr} + c_{12}(\varepsilon_{\theta\theta} + \varepsilon_{zz}) - h_{31}B_z \quad (3.47)$$

$$\sigma_{\theta\theta} = c_{11}\varepsilon_{\theta\theta} + c_{12}(\varepsilon_{rr} + \varepsilon_{zz}) - h_{31}B_z \quad (3.48)$$

$$\sigma_{zz} = c_{11}\varepsilon_{zz} + c_{12}(\varepsilon_{rr} + \varepsilon_{\theta\theta}) - h_{33}B_z \quad (3.49)$$

$$\sigma_{rz} = c_{44}\varepsilon_{rz} - h_{15}B_r \quad (3.50)$$

$$H_r = h_{15}\varepsilon_{rz} + \mu_{11}B_r \quad (3.51)$$

$$H_z = h_{31}(\varepsilon_{rr} + \varepsilon_{\theta\theta}) + h_{33}\varepsilon_{zz} + \mu_{11}B_z \quad (3.52)$$

3.5 Partial Differential Equations

Having defined the appropriate constitutive equations, we next substitute them into the relevant equilibrium equations to extract a system of partial differential equations which must be solved together with the boundary conditions to determine the mechanical and magnetic response to indentation.

3.5.1 Stress and Magnetic Flux Density (σ , B) Representation

Substituting the appropriate constitutive equations, Eqs. 3.26–3.31, into the equilibrium equations, Eqs. 3.5, 3.6, and 3.11, we get

$$\left[c_{11} \frac{\partial \varepsilon_{rr}}{\partial r} + c_{12} \frac{\partial \varepsilon_{\theta\theta}}{\partial r} + c_{13} \frac{\partial \varepsilon_{zz}}{\partial r} - e_{31} \frac{\partial H_z}{\partial r} \right] + \left[c_{44} \frac{\partial \varepsilon_{rz}}{\partial z} - e_{15} \frac{\partial H_r}{\partial z} \right] + \left[\frac{c_{11} - c_{12}}{r} (\varepsilon_{rr} - \varepsilon_{\theta\theta}) \right] = 0$$

$$\left[c_{44} \frac{\partial \varepsilon_{rz}}{\partial r} - e_{15} \frac{\partial H_r}{\partial r} \right] + \left[c_{13} \left(\frac{\partial \varepsilon_{rr}}{\partial z} + \frac{\partial \varepsilon_{\theta\theta}}{\partial z} \right) + c_{33} \frac{\partial \varepsilon_{zz}}{\partial z} - e_{33} \frac{\partial H_z}{\partial z} \right] + \left[c_{44} \frac{\varepsilon_{rz}}{r} - e_{15} \frac{H_r}{r} \right] = 0$$

$$\left[e_{15} \frac{\partial \varepsilon_{rz}}{\partial r} + \mu_{11} \frac{\partial H_r}{\partial r} \right] + \left[\frac{1}{r} (e_{15}\varepsilon_{rz} + \mu_{11}H_r) \right] + \left[e_{31} \left(\frac{\partial \varepsilon_{rr}}{\partial z} + \frac{\partial \varepsilon_{\theta\theta}}{\partial z} \right) + e_{33} \frac{\partial \varepsilon_{zz}}{\partial z} \right] = 0$$

Substituting in the small-strain equations, Eqs. 3.7–3.10, leads to the three partial differential equations which must be solved:

$$c_{11} \left(\frac{\partial^2 u_r}{\partial r^2} + \frac{1}{r} \frac{\partial u_r}{\partial r} - \frac{u_r}{r^2} \right) + c_{44} \frac{\partial^2 u_r}{\partial z^2} + (c_{13} + c_{44}) \frac{\partial^2 u_z}{\partial r \partial z} - e_{15} \frac{\partial H_r}{\partial z} - e_{31} \frac{\partial H_z}{\partial r} = 0 \quad (3.53)$$

$$c_{44} \left(\frac{\partial^2 u_z}{\partial r^2} + \frac{1}{r} \frac{\partial u_z}{\partial r} \right) + c_{33} \frac{\partial^2 u_z}{\partial z^2} + (c_{13} + c_{44}) \frac{\partial}{\partial z} \left(\frac{\partial u_r}{\partial r} + \frac{u_r}{r} \right) - e_{15} \left(\frac{\partial H_r}{\partial r} + \frac{H_r}{r} \right) - e_{33} \frac{\partial H_z}{\partial z} = 0 \quad (3.54)$$

$$e_{15} \left(\frac{\partial^2 u_z}{\partial r^2} + \frac{1}{r} \frac{\partial u_z}{\partial r} \right) + e_{33} \frac{\partial^2 u_z}{\partial z^2} + (e_{15} + e_{31}) \frac{\partial}{\partial z} \left(\frac{\partial u_r}{\partial r} + \frac{u_r}{r} \right) + \mu_{11} \left(\frac{\partial H_r}{\partial r} + \frac{H_r}{r} \right) + \mu_{33} \frac{\partial H_z}{\partial z} = 0 \quad (3.55)$$

An additional constraint is needed since these three partial differential equations contain four variables ($u_r, u_z, H_r,$ and H_z). One way to resolve this is to use the magnetic scalar potential described in Section 3.3.2: $\vec{H} = -\nabla\phi_M$.

$$c_{11} \left(\frac{\partial^2 u_r}{\partial r^2} + \frac{1}{r} \frac{\partial u_r}{\partial r} - \frac{u_r}{r^2} \right) + c_{44} \frac{\partial^2 u_r}{\partial z^2} + (c_{13} + c_{44}) \frac{\partial^2 u_z}{\partial r \partial z} - e_{15} \frac{\partial^2 \phi_M}{\partial z \partial r} - e_{31} \frac{\partial^2 \phi_M}{\partial r \partial z} = 0 \quad (3.56)$$

$$c_{44} \left(\frac{\partial^2 u_z}{\partial r^2} + \frac{1}{r} \frac{\partial u_z}{\partial r} \right) + c_{33} \frac{\partial^2 u_z}{\partial z^2} + (c_{13} + c_{44}) \frac{\partial}{\partial z} \left(\frac{\partial u_r}{\partial r} + \frac{u_r}{r} \right) - e_{15} \left(\frac{\partial^2 \phi_M}{\partial r^2} + \frac{1}{r} \frac{\partial \phi_M}{\partial r} \right) - e_{33} \frac{\partial^2 \phi_M}{\partial z^2} = 0 \quad (3.57)$$

$$e_{15} \left(\frac{\partial^2 u_z}{\partial r^2} + \frac{1}{r} \frac{\partial u_z}{\partial r} \right) + e_{33} \frac{\partial^2 u_z}{\partial z^2} + (e_{15} + e_{31}) \frac{\partial}{\partial z} \left(\frac{\partial u_r}{\partial r} + \frac{u_r}{r} \right) + \mu_{11} \left(\frac{\partial^2 \phi_M}{\partial r^2} + \frac{1}{r} \frac{\partial \phi_M}{\partial r} \right) + \mu_{33} \frac{\partial^2 \phi_M}{\partial z^2} = 0 \quad (3.58)$$

3.5.1.1 Isotropic Material

Following the procedure as above (taking the equilibrium equations, substituting in the above constitutive equations and the small-strain equations), the three partial differential equations become

$$c_{11} \left(\frac{\partial^2 u_r}{\partial r^2} + \frac{1}{r} \frac{\partial u_r}{\partial r} - \frac{u_r}{r^2} \right) + c_{44} \frac{\partial^2 u_r}{\partial z^2} + (c_{12} + c_{44}) \frac{\partial^2 u_z}{\partial r \partial z} - e_{15} \frac{\partial^2 \phi_M}{\partial z \partial r} - e_{31} \frac{\partial^2 \phi_M}{\partial r \partial z} = 0 \quad (3.59)$$

$$c_{44} \left(\frac{\partial^2 u_z}{\partial r^2} + \frac{1}{r} \frac{\partial u_z}{\partial r} \right) + c_{11} \frac{\partial^2 u_z}{\partial z^2} + (c_{12} + c_{44}) \frac{\partial}{\partial z} \left(\frac{\partial u_r}{\partial r} + \frac{u_r}{r} \right) - e_{15} \left(\frac{\partial^2 \phi_M}{\partial r^2} + \frac{1}{r} \frac{\partial \phi_M}{\partial r} \right) - e_{33} \frac{\partial^2 \phi_M}{\partial z^2} = 0 \quad (3.60)$$

$$e_{15} \left(\frac{\partial^2 u_z}{\partial r^2} + \frac{1}{r} \frac{\partial u_z}{\partial r} \right) + e_{33} \frac{\partial^2 u_z}{\partial z^2} + (e_{15} + e_{31}) \frac{\partial}{\partial z} \left(\frac{\partial u_r}{\partial r} + \frac{u_r}{r} \right) + \mu_{11} \left(\frac{\partial^2 \phi_M}{\partial r^2} + \frac{1}{r} \frac{\partial \phi_M}{\partial r} + \frac{\partial^2 \phi_M}{\partial z^2} \right) = 0 \quad (3.61)$$

We can rewrite these equations using the more widely used Young's modulus E , shear modulus G , and Poisson ratio ν as shown in Eq. 3.38, and then they are:

$$\frac{E(1-\nu)}{(1+\nu)(1-2\nu)} \left(\frac{\partial^2 u_r}{\partial r^2} + \frac{1}{r} \frac{\partial u_r}{\partial r} - \frac{u_r}{r^2} \right) + \frac{E}{2(1+\nu)} \frac{\partial^2 u_r}{\partial z^2} + \left(\frac{E}{2(1+\nu)(1-2\nu)} \right) \frac{\partial^2 u_z}{\partial r \partial z} - e_{15} \frac{\partial^2 \phi_M}{\partial z \partial r} - e_{31} \frac{\partial^2 \phi_M}{\partial r \partial z} = 0 \quad (3.62)$$

$$\frac{E}{2(1+\nu)} \left(\frac{\partial^2 u_z}{\partial r^2} + \frac{1}{r} \frac{\partial u_z}{\partial r} \right) + \frac{E(1-\nu)}{(1+\nu)(1-2\nu)} \frac{\partial^2 u_z}{\partial z^2} + \left(\frac{E}{2(1+\nu)(1-2\nu)} \right) \frac{\partial}{\partial z} \left(\frac{\partial u_r}{\partial r} + \frac{u_r}{r} \right) - e_{15} \left(\frac{\partial^2 \phi_M}{\partial r^2} + \frac{1}{r} \frac{\partial \phi_M}{\partial r} \right) - e_{33} \frac{\partial^2 \phi_M}{\partial z^2} = 0 \quad (3.63)$$

$$e_{15} \left(\frac{\partial^2 u_z}{\partial r^2} + \frac{1}{r} \frac{\partial u_z}{\partial r} \right) + e_{33} \frac{\partial^2 u_z}{\partial z^2} + (e_{15} + e_{31}) \frac{\partial}{\partial z} \left(\frac{\partial u_r}{\partial r} + \frac{u_r}{r} \right) + \mu_{11} \left(\frac{\partial^2 \phi_M}{\partial r^2} + \frac{1}{r} \frac{\partial \phi_M}{\partial r} + \frac{\partial^2 \phi_M}{\partial z^2} \right) = 0 \quad (3.64)$$

which contain only 5 constants. Note that the denominator in Eqs. 3.62 and 3.63 contains the term $1 - 2\nu$. Later, we will take advantage of this to simplify the PDEs for the case of an incompressible material ($\nu = 0.5$).

3.5.2 PDEs in the (σ, H) Representation

Using the same equilibrium equations as above results in a set of PDE's which are almost identical to Eqs. 3.62–3.64 (except that the H_i become B_i and e_{jk} become h_{jk}). Alternatively, treating the magnetostrictive case in analogy to the piezoelectric case (this includes treating the electrostatic and magnetostatic equilibrium equations which are both equal to zero as analogous), would dictate using $\vec{\nabla} \times \vec{H} = \vec{J}_{free}$, which is the equivalent to $\vec{\nabla} \cdot \vec{D} = \rho$, instead of $\vec{\nabla} \cdot \vec{B} = 0$. In the piezoelectric case ρ was set equal to zero, but that can not automatically be done for the magnetostrictive case. By not applying any magnetic field and by indenting slowly (much slower than the speed of sound in the material; i.e., so as not to cause rapid changes in magnetization), however, it can be assumed that $\vec{J}_{free} = 0$. Note that $J_z = 0$ for a non-conducting indenter.

3.5.2.1 General Case: Cylindrical Symmetry

Following the discussion above, we can repeat the analysis for the general case. The only difference is that these equations are derived from Eqs. 3.41–3.46 and Eqs. 3.12–3.14 instead of Eq. 3.11 (i.e., Ampère's law instead of the conservation of magnetic flux law). No currents are applied in the experiments, and so $\vec{J}_{free} = 0$. Specifically, by using a non-conducting indenter, we can force $J_z = 0$ at the surface. Then,

$$c_{11} \left(\frac{\partial^2 u_r}{\partial r^2} + \frac{1}{r} \frac{\partial u_r}{\partial r} - \frac{u_r}{r^2} \right) + c_{44} \frac{\partial^2 u_r}{\partial z^2} + (c_{13} + c_{44}) \frac{\partial^2 u_z}{\partial r \partial z} - h_{15} \frac{\partial B_r}{\partial z} - h_{31} \frac{\partial B_z}{\partial r} = 0 \quad (3.65)$$

$$c_{44} \left(\frac{\partial^2 u_z}{\partial r^2} + \frac{1}{r} \frac{\partial u_z}{\partial r} \right) + c_{33} \frac{\partial^2 u_z}{\partial z^2} + (c_{13} + c_{44}) \frac{\partial}{\partial z} \left(\frac{\partial u_r}{\partial r} + \frac{u_r}{r} \right) - h_{15} \left(\frac{\partial B_r}{\partial r} + \frac{B_r}{r} \right) - h_{33} \frac{\partial B_z}{\partial z} = 0 \quad (3.66)$$

$$h_{15} \frac{1}{r} \left(\frac{\partial^2 u_r}{\partial r \partial z} + \frac{\partial^2 u_z}{\partial r^2} \right) - \nu_{11} \frac{1}{r} \frac{\partial B_r}{\partial r} = 0 \quad (3.67)$$

$$-(h_{15} + h_{33}) \frac{\partial^2 u_z}{\partial r \partial z} + h_{31} \left(\frac{\partial^2 u_r}{\partial r^2} + \frac{1}{r} \frac{\partial u_r}{\partial r} - \frac{u_r}{r^2} \right) - h_{15} \frac{\partial^2 u_r}{\partial z^2} + \nu_{11} \frac{\partial B_r}{\partial z} + \nu_{33} \frac{\partial B_z}{\partial r} = 0 \quad (3.68)$$

Note that we now avoid the problem we faced before: We have four equations for four unknowns (u_r, u_z, B_r, B_z) .

3.5.2.2 Isotropic Material

As in the last section, these partial differential equations simplify greatly under the assumption of isotropy.

$$c_{11} \left(\frac{\partial^2 u_r}{\partial r^2} + \frac{1}{r} \frac{\partial u_r}{\partial r} - \frac{u_r}{r^2} \right) + c_{44} \frac{\partial^2 u_r}{\partial z^2} + (c_{12} + c_{44}) \frac{\partial^2 u_z}{\partial r \partial z} - h_{15} \frac{\partial B_r}{\partial z} - h_{31} \frac{\partial B_z}{\partial r} = 0 \quad (3.69)$$

$$c_{44} \left(\frac{\partial^2 u_z}{\partial r^2} + \frac{1}{r} \frac{\partial u_z}{\partial r} \right) + c_{11} \frac{\partial^2 u_z}{\partial z^2} + (c_{12} + c_{44}) \frac{\partial}{\partial z} \left(\frac{\partial u_r}{\partial r} + \frac{u_r}{r} \right) - h_{15} \left(\frac{\partial B_r}{\partial r} + \frac{B_r}{r} \right) - h_{33} \frac{\partial B_z}{\partial z} = 0 \quad (3.70)$$

$$h_{15} \frac{1}{r} \left(\frac{\partial^2 u_r}{\partial r \partial z} + \frac{\partial^2 u_z}{\partial r^2} \right) - \nu_{11} \frac{1}{r} \frac{\partial B_r}{\partial r} = 0 \quad (3.71)$$

$$-(h_{15} + h_{33}) \frac{\partial^2 u_z}{\partial r \partial z} + h_{31} \left(\frac{\partial^2 u_r}{\partial r^2} + \frac{1}{r} \frac{\partial u_r}{\partial r} - \frac{u_r}{r^2} \right) - h_{15} \frac{\partial^2 u_r}{\partial z^2} + \nu_{11} \left(\frac{\partial B_r}{\partial z} + \frac{\partial B_z}{\partial r} \right) = 0 \quad (3.72)$$

Using the stiffness constants relations, Eq. 3.38, we can rewrite the above as

$$\frac{E}{1+\nu} \left[\frac{(1-\nu)}{(1-2\nu)} \left(\frac{\partial^2 u_r}{\partial r^2} + \frac{1}{r} \frac{\partial u_r}{\partial r} - \frac{u_r}{r^2} \right) + \frac{1}{2} \frac{\partial^2 u_r}{\partial z^2} + \frac{1}{2(1-2\nu)} \frac{\partial^2 u_z}{\partial r \partial z} \right] - h_{15} \frac{\partial B_r}{\partial z} - h_{31} \frac{\partial B_z}{\partial r} = 0 \quad (3.73)$$

$$\frac{E}{1+\nu} \left[\frac{1}{2} \left(\frac{\partial^2 u_z}{\partial r^2} + \frac{1}{r} \frac{\partial u_z}{\partial r} \right) + \frac{(1-\nu)}{(1-2\nu)} \frac{\partial^2 u_z}{\partial z^2} + \frac{1}{2(1-2\nu)} \frac{\partial}{\partial z} \left(\frac{\partial u_r}{\partial r} + \frac{u_r}{r} \right) \right] - h_{15} \left(\frac{\partial B_r}{\partial r} + \frac{B_r}{r} \right) - h_{33} \frac{\partial B_z}{\partial z} = 0 \quad (3.74)$$

$$h_{15} \frac{1}{r} \left(\frac{\partial^2 u_r}{\partial r \partial z} + \frac{\partial^2 u_z}{\partial r^2} \right) - \nu_{11} \frac{1}{r} \frac{\partial B_r}{\partial r} = 0 \quad (3.75)$$

$$-(h_{15} + h_{33}) \frac{\partial^2 u_z}{\partial r \partial z} + h_{31} \left(\frac{\partial^2 u_r}{\partial r^2} + \frac{1}{r} \frac{\partial u_r}{\partial r} - \frac{u_r}{r^2} \right) - h_{15} \frac{\partial^2 u_r}{\partial z^2} + \nu_{11} \left(\frac{\partial B_r}{\partial z} + \frac{\partial B_z}{\partial r} \right) = 0 \quad (3.76)$$

3.6 Boundary Conditions

The magnetic boundary conditions are continuity equations, i.e., instead of absolute boundary conditions (e.g. $H = 0$ at some position), they only the fields on either side of a boundary.

3.6.1 Mechanical

We invoke the standard assumptions for mechanical boundary conditions under a spherical indenter.

First, assume that the displacements go to zero far away from the indenter:

$$u_r, u_z \rightarrow \frac{1}{\sqrt{r^2 + z^2}} \quad \text{as} \quad \sqrt{r^2 + z^2} \rightarrow \infty \quad (3.77)$$

Second, assume a rigid indenter (i.e., the indenter head doesn't deform):

$$u_z(r, 0) = h - \frac{r^2}{D} \quad \forall \quad 0 \leq r < a \quad (3.78)$$

Third, assume that the contact is frictionless:

$$\sigma_{rz}(r, 0) = 0 \quad \forall \quad r \geq 0 \quad (3.79)$$

Finally, assume there are no other normal forces outside of the indenter contact area:

$$\sigma_{zz}(r, 0) = 0 \quad \forall \quad r > a \quad (3.80)$$

3.6.2 Magnetic

Let subscript 1 refer to the indenter, and subscript 2, the indented substrate. The general magnetic boundary conditions are

$$B_{1\text{normal}} = B_{2\text{normal}} \quad (3.81)$$

$$H_{1\text{tangent}} = H_{2\text{tangent}} \quad (3.82)$$

which state that the normal component of the magnetic flux density B is continuous across an interface, as is the tangential component of the magnetic field H .

Referring to Figure 1-4, at the top and bottom of the body, using Eq. 3.81 (the surface normal continuity condition), we see that

$$\mu_0 H_{z\text{air}} = \mu_r \mu_0 H_{z\text{material}} + e_{31}(\varepsilon_{rr} + \varepsilon_{\theta\theta}) + e_{33}\varepsilon_{zz} \quad (3.83)$$

where the last two terms are the change in magnetization part of B . At the sides,

$$\mu_0 H_{r\text{air}} = \mu_r \mu_0 H_{r\text{material}} + e_{15}\varepsilon_{rz} \quad (3.84)$$

Because the displacements (and therefore the strains) vanish far away from the indenter (within a distance 7 to 10 times the contact radius), the strain components above vanish, and the above conditions become *at the sides and the bottom* (not near the indenter on top)

$$\mu_0 H_{n\text{air}} = \mu_r \mu_0 H_{n\text{material}} \quad (3.85)$$

One notable feature of Eq. 3.82 is that at the interface between two materials with a large permeability difference, the magnetic flux density vector in the lower permeability material is nearly normal to the interface. Equation 3.82 gives

$$\frac{B_{1\text{tangent}}}{\mu_1} = \frac{B_{2\text{tangent}}}{\mu_2} \quad (3.86)$$

from which it is seen that $B_{2\text{tangent}} \rightarrow 0$ when $\mu_1 \gg \mu_2$. Physical arguments (and conservation of energy) show that $H \rightarrow 0$ as $r, z \rightarrow \infty$.

As shown in Section 3.3.2.1, $H_\theta = 0$. For a non-conducting indenter, $J_z = 0$; therefore at the surface (from Eq. 3.14)

$$\frac{1}{r} \frac{\partial H_r}{\partial r} = 0 \quad (3.87)$$

3.6.2.1 Incompressible Material

As will be seen in Section 3.7.1, the case for an incompressible material (i.e., one for which $\nu = 0.5$) is a special limiting case that is relatively easy to solve. The results from this case can be used as a guide to the more general solution. The magnetic boundary condition on the surface near the indenter, Eq. 3.83, will simplify in the case of an incompressible material as follows. Because $\varepsilon_{rr} + \varepsilon_{\theta\theta} + \varepsilon_{zz} = 0$ for $\nu = 0.5$, Eq. 3.83 becomes

$$\mu_0 H_{z\text{air}} = \mu_r \mu_0 H_{z\text{material}} + (e_{33} - e_{31}) \varepsilon_{zz} \quad (3.88)$$

At $r = 0$ on the surface, $\varepsilon_{zz} = 0$ (in the pure mechanical case), and so this boundary condition is greatly simplified. In fact, it is no longer useful in solving the general material response equations; it is an “output” function which tells us how the magnetic field changes at the surface. Equation 3.88 is, however, useful in the experimental measurements. The above condition could also be assumed for the case of near-incompressibility.

3.7 Solution

A solution for the stress/magnetic flux density (σ, B) representation only is detailed here. The solution presented is applicable at the surface of the body only, for reasons which are discussed below.

3.7.1 Particular Solution: Isotropic, Incompressible ($\nu = 0.5$) Solid

Starting with the isotropic partial differential equations from Sec. 3.5.1, in the limit as ν goes to 0.5 (i.e., as we approach the ideal of an incompressible solid)³, the constitutive equations can be simplified (by multiplying both sides by the term $(1 - 2\nu)$ and letting $\nu = 0.5$) to

$$0 = \frac{E(1-\nu)}{1+\nu} \left(\frac{\partial^2 u_r}{\partial r^2} + \frac{1}{r} \frac{\partial u_r}{\partial r} - \frac{u_r}{r^2} \right) + \frac{E}{2(1+\nu)} \frac{\partial^2 u_z}{\partial r \partial z} \quad (3.89)$$

$$0 = \frac{E(1-\nu)}{1+\nu} \frac{\partial^2 u_z}{\partial z^2} + \frac{E}{2(1+\nu)} \frac{\partial}{\partial z} \left(\frac{\partial u_r}{\partial r} + \frac{u_r}{r} \right) \quad (3.90)$$

$$0 = e_{15} \left(\frac{\partial^2 u_z}{\partial r^2} + \frac{1}{r} \frac{\partial u_z}{\partial r} \right) + e_{33} \frac{\partial^2 u_z}{\partial z^2} + (e_{15} + e_{31}) \frac{\partial}{\partial z} \left(\frac{\partial u_r}{\partial r} + \frac{u_r}{r} \right) + \mu_{11} \left(\frac{\partial H_r}{\partial r} + \frac{H_r}{r} + \frac{\partial H_z}{\partial z} \right) \quad (3.91)$$

Eqs. 3.89 and 3.90 should in fact lead to the classical indentation solutions of u_r and u_z for a spherical indenter, because the magnetoelastic coupling has been removed from these equations by virtue of letting ν go to 0.5. The only remaining coupling is in Eq. 3.91, and it is weaker than in the general case. Since $\varepsilon_{rr} + \varepsilon_{\theta\theta} + \varepsilon_{zz} = 0$ for an incompressible solid, we can replace Eq. 3.91 with the following:

$$0 = e_{15} \left(\frac{\partial^2 u_z}{\partial r^2} + \frac{1}{r} \frac{\partial u_z}{\partial r} \right) + (e_{33} - e_{15} - e_{31}) \frac{\partial^2 u_z}{\partial z^2} + \mu_{11} \left(\frac{\partial H_r}{\partial r} + \frac{H_r}{r} + \frac{\partial H_z}{\partial z} \right) \quad (3.92)$$

Besides being the solution for the idealized case of an incompressible material, this may be useful when dealing with composites, where a magnetostrictive material would be combined with, perhaps, a rubber or other material with ν close to 0.5, and for cases where ν approaches 0.5, like Terfenol-D.

3.7.1.1 Homogeneous Solution

Since Eqs. 3.89–3.90 will result in the classical indentation solution, u_r and u_z are already known, and only H_r and H_z remain to be solved. First, the general solution for the homogeneous case is obtained. Remembering that $\vec{H} = -\nabla\phi_M$, the homogeneous portion of Eq. 3.92 is

$$\frac{\partial^2 \phi_M}{\partial r^2} + \frac{1}{r} \frac{\partial \phi_M}{\partial r} + \frac{\partial^2 \phi_M}{\partial z^2} = 0 \quad (3.93)$$

³Incompressible materials exhibit conservation of volume, and thus $\varepsilon_{31} = -\varepsilon_{33}/2$. The mechanical and magnetic behavior should almost completely decouple, then, because $e_{31} = -e_{33}/2$.

Using separation of variables, we let $\phi_M = R(r)Z(z)$, where R and Z are functions solely of r and z , respectively. Then we arrive at the two following ordinary differential equations:

$$\frac{d^2 R}{dr^2} + \frac{1}{r} \frac{dR}{dr} = +\lambda R \quad (3.94)$$

$$\frac{d^2 Z}{dz^2} = -\lambda Z \quad (3.95)$$

The sign of λ determines the type of solution. Equation 3.94 is in the form of Bessel's equations, and results in either the regular or the modified Bessel functions, depending on λ . Eq. 3.95 results in either an exponential solution or a sine and cosine solution, again depending on the sign of λ . For $\lambda < 0$, the solutions are

$$R(r) = \sum_{n=1}^{\infty} \left(s_{1n} J_0 \left[r\sqrt{-\lambda_n} \right] + s_{2n} K_0 \left[r\sqrt{\lambda_n} \right] \right) \quad (3.96)$$

$$Z(z) = \sum_{n=1}^{\infty} \left(s_{3n} \exp \left(-z\sqrt{-\lambda_n} \right) + s_{4n} \exp \left(z\sqrt{-\lambda_n} \right) \right) \quad (3.97)$$

where $J_n[x]$ and $K_n[x]$ are the Bessel function of the first kind and the modified Bessel function of the second kind, respectively⁴. For $\lambda > 0$, the solutions are

$$R(r) = \sum_{n=1}^{\infty} \left(s_{1n} I_0 \left[r\sqrt{\lambda_n} \right] + s_{2n} K_0 \left[r\sqrt{\lambda_n} \right] \right) \quad (3.98)$$

$$Z(z) = \sum_{n=1}^{\infty} \left(s_{3n} \cos \left(z\sqrt{\lambda_n} \right) + s_{4n} \sin \left(z\sqrt{\lambda_n} \right) \right) \quad (3.99)$$

and from dimensional arguments, we set $\lambda_n \propto \pm \frac{1}{a^2}$.

For reasons which will become apparent later, we use the solution for $\lambda < 0$ for the region inside the contact radius, $r < a$, and the solution for $\lambda > 0$ for the region outside, $r > a$. By imposing continuity at $r = a$, these solutions become continuous functions.

3.7.1.2 Non-Homogeneous Solution

The non-homogeneous part of Eq. 3.92 is

$$e_{15} \left(\frac{\partial^2 u_z}{\partial r^2} + \frac{1}{r} \frac{\partial u_z}{\partial r} \right) + \left(\frac{3}{2} e_{33} - e_{15} \right) \frac{\partial^2 u_z}{\partial z^2}$$

⁴Bessel functions are solutions to the equation $z^2 y'' + zy' + (z^2 - n^2)y = 0$. The functions are referred to as Bessel functions of the first and second kind, $J_n[x]$ and $Y_n[x]$ respectively. Modified Bessel functions are solutions to the equation $z^2 y'' + zy' - (z^2 + n^2)y = 0$. The functions are referred to as modified Bessel functions of the first and second kind, $I_n[x]$ and $K_n[x]$ respectively. For the case presented here, $n = 0$.

This is functionally dependent only on u_z — namely on its first derivative with respect to r as well as its second derivatives with respect to r and with respect to z . An analytic form for u_z at the surface ($z = 0$) is given in Johnson [8] (see Appendix A for details). This form, however, has no dependence on z , and so we can not use it to evaluate $\partial u_z / \partial z$ or $\partial^2 u_z / \partial z^2$ (and we will have to be cautious about its applicability to $\partial u_z / \partial r$ because we may want u_z as a function of r and z). We therefore need to evaluate the full functional dependence of u_z near the surface.

The displacement along the z direction, u_z , can be determined in a number of ways — methods discussed in Hamilton [18] and Johnson [8] are two examples. Numerical integration using the potential method presented by Johnson [8, pp. 45–50] is the most straightforward. For the case of a frictionless contact,

$$\Psi = \iint_S \frac{p(\xi, \eta)}{\rho} d\xi d\eta \quad (3.100)$$

where $p(\xi, \eta)$ is the pressure distribution over the contact area, S is the contact area, and ρ is the distance from a point in the contact area to any point in the body. For Hertzian pressure distribution and a cylindrical coordinate system, the integral is

$$\Psi = \iint_S \frac{p(r_2, \theta_2)}{\rho} r_2 dr_2 d\theta_2 = \int_0^{2\pi} \int_0^a \frac{Pr_2 \sqrt{1 - \frac{r_2^2}{a^2}}}{\sqrt{z^2 + r_1^2 + r_2^2 - 2r_1 r_2 \cos(\theta_1 - \theta_2)}} dr_2 d\theta_2 \quad (3.101)$$

where P is the total applied load, r_1 and θ_1 are coordinates for a point inside the contact area, and r_2, z and θ_2 are coordinates for a point inside the body of the solid. We use Ψ to find u_z :

$$u_z = \frac{1}{4\pi G} \left(2(1 - \nu)\Psi - z \frac{\partial \Psi}{\partial z} \right) \quad (3.102)$$

where G is the shear modulus.

The numerical integration to evaluate u_z and subsequent numerical derivatives show that $\partial^2 u_z / \partial z^2$ is effectively zero at the surface ($z = 0$), and therefore the middle term in Eq. 3.92 is zero and can therefore be ignored. Eq. 3.92 then becomes

$$0 = e_{15} \left(\frac{\partial^2 u_z}{\partial r^2} + \frac{1}{r} \frac{\partial u_z}{\partial r} \right) + \mu_{11} \left(\frac{\partial H_r}{\partial r} + \frac{H_r}{r} + \frac{\partial H_z}{\partial z} \right) \quad (3.103)$$

In order to simplify notation later on, we set

$$\Xi = \mu_{11} \left(\frac{\partial H_r}{\partial r} + \frac{H_r}{r} + \frac{\partial H_z}{\partial z} \right) \quad (3.104)$$

$$\Gamma = -e_{15} \left(\frac{\partial^2 u_z}{\partial r^2} + \frac{1}{r} \frac{\partial u_z}{\partial r} \right) \quad (3.105)$$

If $e_{15} = 0$, then the system is completely decoupled: the third partial differential equation, Eq. 3.92, reduces to solely magnetic terms (which were in turn derived from the magnetic divergence equation). Then we have an infinite set of possible solutions; but with no “driving force,” the trivial solution (with all magnetic fields equal to zero) is the only one left.

Note that this result highlights the importance of e_{15} , a constant which is generally not reported in the literature (except for the reference discussed in Chapter 2 and general descriptions of e_{15} being on the order of one-half of e_{33}).

The numerical integration also shows that near the surface

$$\frac{\partial}{\partial z} \left(\frac{\partial u_z}{\partial r} \right) \approx 0 \quad \text{and} \quad \frac{\partial}{\partial z} \left(\frac{\partial^2 u_z}{\partial r^2} \right) \approx 0 \quad (3.106)$$

Therefore we do not need to use the numerical integration results for u_z but can instead directly use the analytical forms shown in Johnson [8], provided the resulting solution is applied only at $z = 0$.

The z displacements (u_z , see Appendix A, Eqs. A.8 and A.9) for $r < a$ are

$$\begin{aligned} \frac{\partial u_z}{\partial r} &= -\frac{\pi p_0}{2a} \frac{1 - \nu^2}{E} r \\ \frac{\partial^2 u_z}{\partial r^2} &= -\frac{\pi p_0}{2a} \frac{1 - \nu^2}{E} \end{aligned}$$

and so

$$\Gamma_{\text{in}} = -\frac{\pi p_0}{a} \frac{1 - \nu^2}{E^*} e_{15} = -\pi \Theta \quad (3.107)$$

where $\Theta = \frac{1 - \nu^2}{E} \frac{p_0}{a} e_{15}$, E^* is the composite elastic modulus, and p_0 is the maximum contact pressure. Similarly, the z displacements (see Eqs. A.8 and A.9) for $r > a$ are

$$\begin{aligned} \frac{\partial u_z}{\partial r} &= \frac{1 - \nu^2}{E} \frac{p_0}{a} \left(a \sqrt{1 - \frac{a^2}{r^2}} - r \arcsin \left(\frac{a}{r} \right) \right) \\ \frac{\partial^2 u_z}{\partial r^2} &= \frac{1 - \nu^2}{E} \frac{p_0}{a} \left(\frac{a}{r} \frac{1 + \frac{a^2}{r^2}}{\sqrt{1 - \frac{a^2}{r^2}}} - \arcsin \left(\frac{a}{r} \right) \right) \end{aligned}$$

Combining these and switching to the dimensionless radial unit $\gamma = r/a$ gives

$$\Gamma_{\text{out}} = \Theta \left(\frac{a}{r} \frac{2}{\sqrt{1 - \frac{a^2}{r^2}}} - 2 \arcsin \left(\frac{a}{r} \right) \right) = \Theta \left(\frac{2}{\gamma \sqrt{1 - \frac{1}{\gamma^2}}} - 2 \arcsin \left(\frac{1}{\gamma} \right) \right) \quad (3.108)$$

Figure 3-1 shows the plot of Γ both inside and outside the contact radius.

Fields inside the contact radius: When choosing solutions to Eqs. 3.94–3.95, it is apparent that the solutions for $\lambda < 0$ are the most appropriate, because it provides for an exponential decay in z

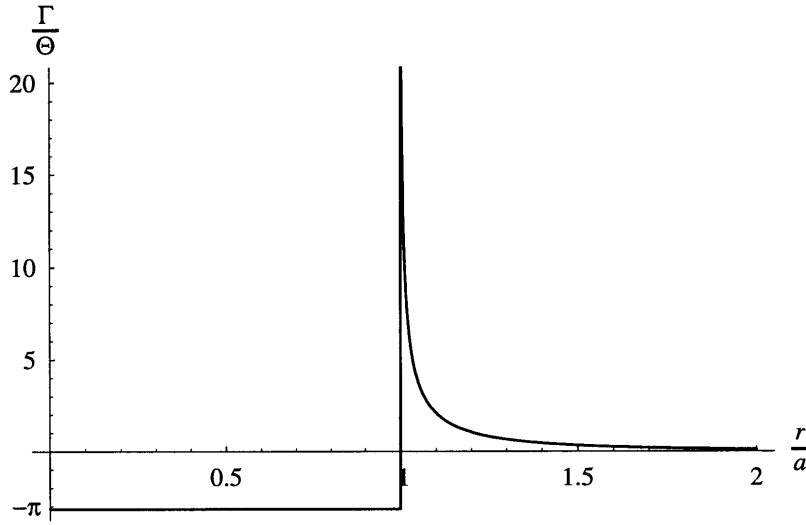


FIGURE 3-1: Plot of the differential function Γ vs. r/a .

and also a strong decay in r — it is obvious that the magnetic field can not continually increase with distance from the point of contact. Because the magnetic field can not go to infinity as $z \rightarrow \infty$, s_{4_n} is immediately zero. Similarly, since the magnetic field should not blow up at $z = 0$, $s_{2_n} = 0$. This leaves a solution which decays exponentially away from the surface, and which has a smooth, well-behaved r dependence near the origin. Because λ_n defines a relevant length scale for each term in the solution series, setting $\lambda_n = -\frac{1}{n^2 a^2}$ is appropriate for the region inside the contact radius, because this defines a set of length scales: $\frac{r}{a}, \frac{1}{2} \frac{r}{a}, \frac{1}{3} \frac{r}{a}, \dots$. Letting $\frac{r}{a} \rightarrow \gamma$, the solution can now be written as

$$\phi_M = R(r)Z(z) = \sum_{n=1}^{\infty} k_{n_{in}} J_0 \left[\frac{\gamma}{n} \right] \exp \left(-\frac{z}{na} \right) \quad (3.109)$$

where $k_{n_{in}} = s_{1_n} \cdot s_{3_n}$.

In order to determine the complete non-homogeneous solution, let $k_{n_{in}}$ become a function of r , then solve $\Gamma_{in} = \Xi_{in}$ for $k_{n_{in}}$. This change in the k_n has implications for calculating H_z , which is defined as $-\partial\phi_M/\partial z$. Applying this definition gives

$$H_z = R(r) \left[k_n \frac{\partial Z(z)}{\partial z} + Z(z) \frac{\partial k_n}{\partial z} \right] \quad (3.110)$$

But, as will be shown below, k_n are solved as functions of r only, and so $\partial k_n/\partial z = 0$. Thus the second term above is zero for this solution. In a more general way, the second term in Eq. 3.110 is expected to be much smaller than the first term, however, and so neglecting it is a good approximation.

The easiest way to solve for the $c_{n_{in}}$ is to approximate Γ_{in} with the appropriate Bessel functions, and then match the coefficients of each Bessel function. For reasons which will be apparent later, the

fitting function is chosen to be

$$\mathcal{F}_{\text{in}} = c_{1\text{in}} (J_0 [\gamma] + J_1 [\gamma]) + c_{2\text{in}} \left(J_0 \left[\frac{\gamma}{2} \right] + J_1 \left[\frac{\gamma}{2} \right] \right) + c_{3\text{in}} \left(J_0 \left[\frac{\gamma}{3} \right] + J_1 \left[\frac{\gamma}{3} \right] \right) \quad (3.111)$$

Finally, solve for the $c_{n\text{in}}$ by requiring the area under the curve as well as the height at two points to be equal for both Γ_{in} and \mathcal{F}_{in} , i.e.,

$$\begin{aligned} \int_0^1 \Gamma_{\text{in}} d\gamma &= \int_0^1 \mathcal{F}_{\text{in}} d\gamma && \text{Area under the curve} \\ \Gamma_{\text{in}}|_{\gamma=0.01} &= \mathcal{F}_{\text{in}}|_{\gamma=0.01} && \text{Height at } r = 0.01a \\ \Gamma_{\text{in}}|_{\gamma=0.99} &= \mathcal{F}_{\text{in}}|_{\gamma=0.99} && \text{Height at } r = 0.99a \end{aligned}$$

See Table 3.1 for the solution. The fit is excellent, as can be seen from the vertical range in Figure 3-2 — the discrepancy is never larger than 0.01%.

Constant	Value
$c_{1\text{in}}$	-1.4242Θ
$c_{2\text{in}}$	11.9915Θ
$c_{3\text{in}}$	-13.7089Θ

TABLE 3.1: Values of the constants for $r < a$.

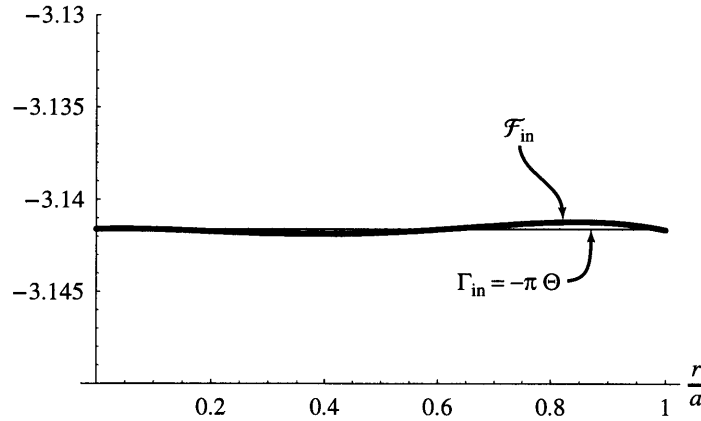


FIGURE 3-2: Comparison of the indentation PDE Γ_{in} to the fitting function \mathcal{F}_{in} .

Returning to the “homogeneous” solution, and letting $z = 0$, the solution for ϕ_M is now

$$\sum_{n=1}^3 k_{n\text{in}} [\gamma] J_0 \left[\frac{\gamma}{n} \right] = k_{1\text{in}} [\gamma] J_0 [\gamma] + k_{2\text{in}} [\gamma] J_0 \left[\frac{\gamma}{2} \right] + k_{3\text{in}} [\gamma] J_0 \left[\frac{\gamma}{3} \right] \quad (3.112)$$

For a given value of n ,

$$\begin{aligned} \frac{\partial^2 \phi_M}{\partial r^2} + \frac{1}{r} \frac{\partial \phi_M}{\partial r} &= \frac{k_n}{r} \frac{\partial J_0}{\partial r} + \frac{J_0}{r} \frac{\partial k_n}{\partial r} + k_n \frac{\partial^2 J_0}{\partial r^2} + 2 \frac{\partial k_n}{\partial r} \frac{\partial J_0}{\partial r} + J_0 \frac{\partial^2 k_n}{\partial r^2} \\ &= \left(\frac{k_n}{r} \frac{\partial J_0}{\partial r} + k_n \frac{\partial^2 J_0}{\partial r^2} \right) + J_0 \left(\frac{1}{r} \frac{\partial k_n}{\partial r} + \frac{\partial^2 k_n}{\partial r^2} \right) + 2 \frac{\partial k_n}{\partial r} \frac{\partial J_0}{\partial r} \end{aligned} \quad (3.113)$$

where the $J_0[\gamma/n]$ has been abbreviated to J_0 . The first two terms are simply the solution of the homogeneous equation, and hence always sum to zero. The last term is the reason why Γ_{in} was approximated with $c_n(J_0 + J_1)$: The first derivative of $J_0[\gamma/n]$ is equal to $-(1/n)J_1[\gamma/n]$. Then the functions $k_{n_{\text{in}}}[\gamma]$ are found by solving the differential equations which result from equating the coefficients in front of Bessel functions (and noting that $\partial\gamma = \frac{1}{a}\partial r$), i.e., by setting $\mathcal{F}_{\text{in}} = \Xi_{\text{in}}$ and matching terms with identical Bessel functions:

$$\frac{1}{ar} \frac{\partial k_{n_{\text{in}}}[\gamma]}{\partial \gamma} + \frac{1}{a^2} \frac{\partial^2 k_{n_{\text{in}}}[\gamma]}{\partial \gamma^2} = \frac{c_{n_{\text{in}}}}{\mu_{11}} \quad (3.114)$$

$$\frac{2}{a} \frac{\partial k_{n_{\text{in}}}[\gamma]}{\partial \gamma} \left(\frac{-1}{an} \right) = \frac{c_{n_{\text{in}}}}{\mu_{11}} \quad (3.115)$$

By treating the equations algebraically, $\frac{\partial k_{n_{\text{in}}}[\gamma]}{\partial \gamma}$ can be solved for in Eq. 3.115 and then substituted back into Eq. 3.114, which results in the differential equation

$$\frac{-nc_{n_{\text{in}}}[\gamma]}{2\gamma\mu_{11}} + \frac{1}{a^2} \frac{\partial^2 k_{n_{\text{in}}}[\gamma]}{\partial \gamma^2} = \frac{c_{n_{\text{in}}}}{\mu_{11}} \quad (3.116)$$

which has a general solution of

$$\frac{1}{\mu_{11}} \left(b_{n_1} + b_{n_2}\gamma - \frac{1}{2}a^2nc_{n_{\text{in}}}\gamma + \frac{a^2c_{n_{\text{in}}}}{2}\gamma^2 + \frac{1}{2}a^2nc_{n_{\text{in}}}\gamma \ln \gamma \right) \quad (3.117)$$

where $b_{n_1} + b_{n_2}\gamma$ is the homogeneous solution, and the remainder is the particular solution. All b_{n_1} and b_{n_2} are set equal to zero, except for b_{11} , which will be used to satisfy the requirement that the magnetic fields must be continuous at $r = a$.

Fields outside the contact radius: Unfortunately, the solution described above is not appropriate for $r > a$, because of the oscillatory behavior of $J_n[r]$. $K_n[r]$ would be a much better solution, given that it decays to zero as $r \rightarrow \infty$, but for $\lambda < 0$ $K_n[r]$ has an imaginary component. Assuming $\lambda > 0$ instead gives the solutions Eqs. 3.98–3.99. Because $I_n[r]$ going to infinity as $r \rightarrow \infty$ is a non-physical solution, $s_{1_n} = 0$. Using a positive value for the λ_n results in a sine and cosine dependence for z , but the solution has already been limited to the region near $z = 0$, so the z dependence is unimportant. Setting $\lambda_n = +\frac{n^2}{a^2}$ is appropriate for the region outside the contact radius, because this defines a set of

length scales: $\frac{r}{a}, 2\frac{r}{a}, 3\frac{r}{a}, \dots$. Again letting $\frac{r}{a} \rightarrow \gamma$, the solution can now be written as

$$\phi_M = R(r)Z(z) = \sum_{n=1}^{\infty} k_{n_{\text{out}}} K_0 [n\gamma] \cos\left(-\frac{nz}{a}\right) \quad (3.118)$$

and we follow the same solution method as above. As can be seen from Figure 3-1, however, the fitting function will need more than three terms in order to closely approximate the behavior of Γ_{out} , given that it goes to infinity at $r = a$ but quickly decays to zero away from the contact radius. Six terms is seen to be adequate for approximating the curve:

$$\begin{aligned} \mathcal{F}_{\text{out}} = & c_{1_{\text{out}}} (K_0 [\gamma] + K_1 [\gamma]) + c_{2_{\text{out}}} (K_0 [2\gamma] + K_1 [2\gamma]) + c_{3_{\text{out}}} (K_0 [3\gamma] + K_1 [3\gamma]) \\ & + c_{4_{\text{out}}} (K_0 [4\gamma] + K_1 [4\gamma]) + c_{5_{\text{out}}} (K_0 [5\gamma] + K_1 [5\gamma]) + c_{6_{\text{out}}} (K_0 [6\gamma] + K_1 [6\gamma]) \end{aligned} \quad (3.119)$$

Then solve for the $c_{n_{\text{out}}}$ by requiring the area under the curve as well as the height at three points as well as the derivative at two points to be equal for both Γ_{out} and \mathcal{F}_{out} , i.e.,

$$\begin{aligned} \int_0^{20} \Gamma_{\text{out}} d\gamma &= \int_0^{20} \mathcal{F}_{\text{out}} d\gamma && \text{Area under the curve} \\ \Gamma_{\text{out}}|_{\gamma=1.04} &= \mathcal{F}_{\text{out}}|_{\gamma=1.04} && \text{Height at } r = 1.04a \\ \Gamma_{\text{out}}|_{\gamma=1.3} &= \mathcal{F}_{\text{out}}|_{\gamma=1.3} && \text{Height at } r = 1.3a \\ \Gamma_{\text{out}}|_{\gamma=2.6} &= \mathcal{F}_{\text{out}}|_{\gamma=2.6} && \text{Height at } r = 2.6a \\ \left. \frac{d\Gamma_{\text{out}}}{dr} \right|_{\gamma=1.3} &= \left. \frac{d\mathcal{F}_{\text{out}}}{dr} \right|_{\gamma=1.3} && \text{Derivative at } r = 1.3a \\ \left. \frac{d\Gamma_{\text{out}}}{dr} \right|_{\gamma=2.6} &= \left. \frac{d\mathcal{F}_{\text{out}}}{dr} \right|_{\gamma=2.6} && \text{Derivative at } r = 2.6a \end{aligned}$$

The upper limit of integration for the integral above would in theory be ∞ , but the fit converges rapidly as seen in Figure 3-3 (and this is expected given that all response decays quickly away from the indentation point), so using an upper limit of $20a$ is perfectly acceptable. The $K_n[x]$ function does not have a singularity at $r=a$ as Γ_1 (the analytical indentation solution) does, so the fit will be non-ideal. The height of the functions were set equal at the two points listed above for the simple reason that these points were those that balanced the singular behavior near $r = a$ with the continually positive value which decayed to zero as $r \rightarrow \infty$. See Table 3.2 for the solution. The fit is quite close, as can be seen from Figure 3-4.

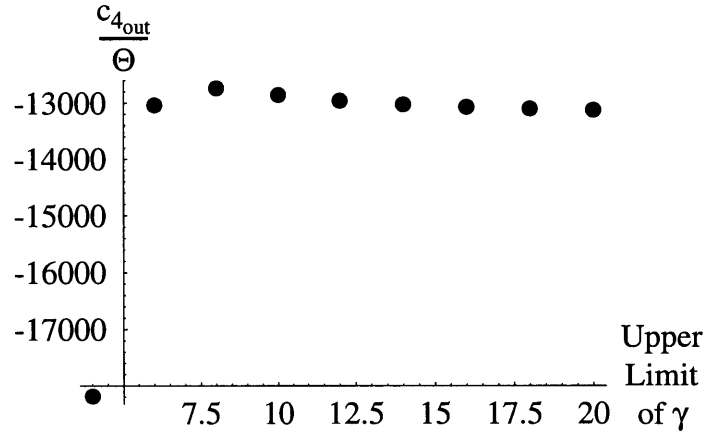


FIGURE 3-3: The value of $c_{4_{out}}/\Theta$ as a function of the upper limit of integration.

Constant	Value
$c_{1_{out}}$	3.3977Θ
$c_{2_{out}}$	-154.82Θ
$c_{3_{out}}$	$2,312.3\Theta$
$c_{4_{out}}$	$-13,117\Theta$
$c_{5_{out}}$	$29,400\Theta$
$c_{6_{out}}$	$-18,715\Theta$

TABLE 3.2: Values of the fitting constants for $r > a$.

Examining the “homogeneous” solution for $r > a$, and letting $z = 0$, it is clear that

$$\sum_{n=1}^6 k_{n_{out}}[\gamma]K_0[n\gamma] = k_{1_{out}}[\gamma]K_0[\gamma] + k_{2_{out}}[\gamma]K_0[2\gamma] + k_{3_{out}}[\gamma]K_0[3\gamma] + k_{4_{out}}[\gamma]K_0[4\gamma] + k_{5_{out}}[\gamma]K_0[5\gamma] + k_{6_{out}}[\gamma]K_0[6\gamma] \tag{3.120}$$

Eq. 3.113 still applies to the $k_{n_{out}}$. Because the basis function is now $K_0[n\gamma]$ instead of $J_0[\gamma/n]$, Eq. 3.115 becomes

$$\frac{2}{a} \frac{\partial k_{n_{out}}[\gamma]}{\partial \gamma} \left(\frac{-1}{a\gamma} \right) = \frac{c_{n_{out}}}{\mu_{11}} \tag{3.121}$$

which modifies Eq. 3.114 as

$$\frac{-c_{n_{out}}[\gamma]}{2n\gamma\mu_{11}} + \frac{1}{a^2} \frac{\partial^2 k_{n_{out}}[\gamma]}{\partial \gamma^2} = \frac{c_{n_{out}}}{\mu_{11}} \tag{3.122}$$

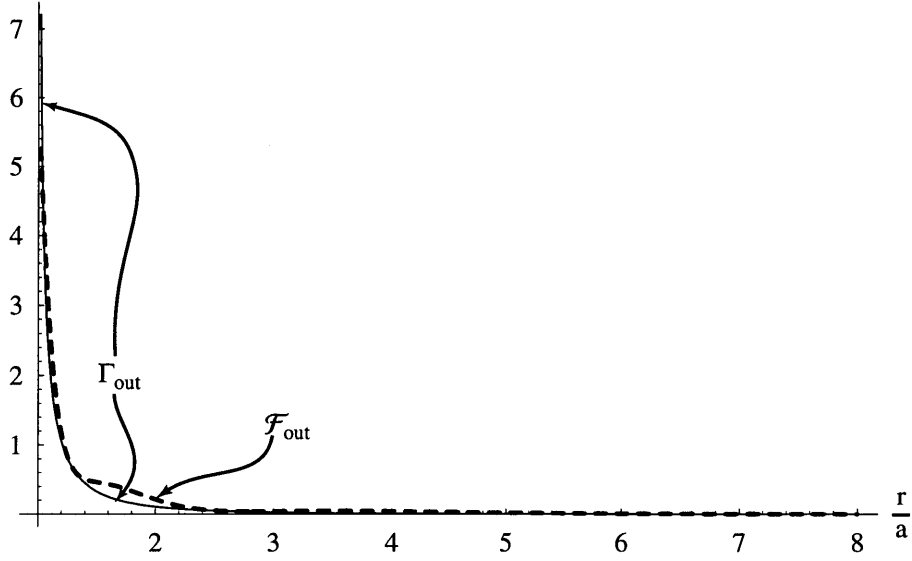


FIGURE 3-4: Comparison of the indentation PDE Γ_{out} to the fitting function \mathcal{F}_{out} .

This equation has the solution of

$$\frac{1}{\mu_{11}} \left(b_{n_1} + b_{n_2} \gamma - \frac{1}{2n} a^2 c_{n_{\text{out}}} \gamma + \frac{a^2 c_{n_{\text{out}}}}{2} \gamma^2 + \frac{1}{2n} a^2 c_{n_{\text{out}}} \gamma \ln \gamma \right) \quad (3.123)$$

where $b_{n_1} + b_{n_2} \gamma$ is the homogeneous solution, and the remainder is the particular solution. Again set all b_{n_1} and b_{n_2} equal to zero, except for b_{1_1} , which will be used to satisfy the requirement that the magnetic fields must be continuous at $r = a$.

Note that the solution both inside and outside the contact radius is given for $z = 0$. A solution as a function of depth in the body (i.e., as a function of z) can be determined by setting z to a non-zero value, evaluating the displacement functions at that value of z , and then reapplying the above method with these new functions.

3.7.2 Complete Solution

Combining the results of the previous section, the solution to the magnetic scalar potential is obtained as follows:

$$\begin{aligned} \mu_{11} \phi_{M_{\text{in}}} = & (b_{1_{\text{in}}} + 0.7121 \Theta a^2 \gamma (1 - \ln[\gamma]) - 0.7121 \Theta a^2 \gamma^2) J_0[\gamma] \exp\left(\frac{-z}{a}\right) \\ & + (-11.992 \Theta a^2 \gamma (1 - \ln[\gamma]) + 5.9958 \Theta a^2 \gamma^2) J_0\left[\frac{\gamma}{2}\right] \exp\left(\frac{-2z}{a}\right) \\ & + (20.563 \Theta a^2 \gamma (1 - \ln[\gamma]) - 6.8545 \Theta a^2 \gamma^2) J_0\left[\frac{\gamma}{3}\right] \exp\left(\frac{-3z}{a}\right) \end{aligned} \quad (3.124)$$

and

$$\begin{aligned}
\mu_{11}\phi_{M_{\text{out}}} = & (b_{1_{\text{out}}} - 1.6847\Theta a^2\gamma(1 - \ln[\gamma]) + 1.6847\Theta a^2\gamma^2) K_0[\gamma] \cos\left(\frac{\pi z}{a}\right) \\
& + (38.327\Theta a^2\gamma(1 - \ln[\gamma]) - 76.654\Theta a^2\gamma^2) K_0[2\gamma] \cos\left(\frac{2\pi z}{a}\right) \\
& + (-381.30\Theta a^2\gamma(1 - \ln[\gamma]) + 1143.9\Theta a^2\gamma^2) K_0[3\gamma] \cos\left(\frac{3\pi z}{a}\right) \\
& + (1619.2\Theta a^2\gamma(1 - \ln[\gamma]) - 6476.9\Theta a^2\gamma^2) K_0[4\gamma] \cos\left(\frac{4\pi z}{a}\right) \\
& + (-2892.9\Theta a^2\gamma(1 - \ln[\gamma]) + 14465\Theta a^2\gamma^2) K_0[5\gamma] \cos\left(\frac{5\pi z}{a}\right) \\
& + (1518.5\Theta a^2\gamma(1 - \ln[\gamma]) - 9111.1\Theta a^2\gamma^2) K_0[6\gamma] \cos\left(\frac{6\pi z}{a}\right)
\end{aligned} \tag{3.125}$$

By requiring that the magnetic fields be continuous at the contact radius, i.e.,

$$\left. \frac{\partial \phi_{M_{\text{in}}}}{\partial r} \right|_{r=a} = \left. \frac{\partial \phi_{M_{\text{out}}}}{\partial r} \right|_{r=a} \quad \text{and} \quad \left. \frac{\partial \phi_{M_{\text{in}}}}{\partial z} \right|_{r=a} = \left. \frac{\partial \phi_{M_{\text{out}}}}{\partial z} \right|_{r=a} \tag{3.126}$$

the remaining two constants are determined to be $b_{1_{\text{in}}} = -10.193\Theta a^2$ and $b_{1_{\text{out}}} = -2.1304\Theta a^2$.

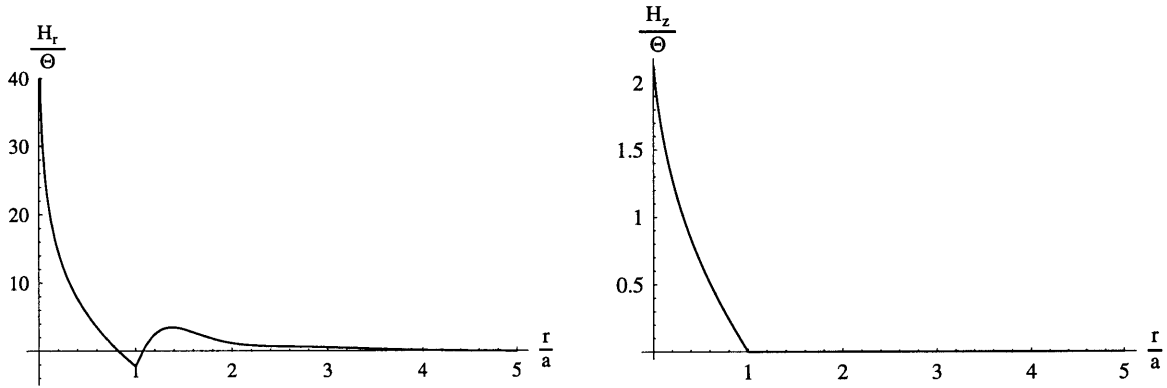


FIGURE 3-5: The final form of a) H_r and b) H_z at $z = 0$ with the constants solved as above.

3.8 Measureable Quantities

Given the experimental geometry (see Section 1.4), the most feasible way of measuring magnetic response is to place a small pickup coil on the sample, centered under the indenter. This enables the detection of the change in flux Φ as a voltage (see Eq. 1.5). The results of Section 3.7 can be compared to the experimental results.

To measure the magnetic field, then, we need to know the relation between the magnetic flux and our computed quantity, H . For a pickup coil positioned on top of the sample (see Chapter 4), the flux Φ_z is

$$\Phi_z = \int_A \vec{B} \cdot d\vec{A} = \int_0^{2\pi} \int_{r_1}^{r_2} \mu_r \mu_0 H_z r \, dr \, d\theta \quad (3.127)$$

where r_1 and r_2 define the region inside the flux pickup coil being integrated. Because there is no dependence on θ , this simplifies to

$$\Phi_z = 2\pi\mu_{11} \int_{r_1}^{r_2} H_z r \, dr = 2\pi\mu_{11} \left(\int_0^a H_{z_{\text{in}}} r \, dr + \int_a^{r_2} H_{z_{\text{out}}} r \, dr \right) \quad (3.128)$$

3.8.1 Isotropic, Incompressible Material

An analytical solution to Eq. 3.127 using the solution for \vec{H} from Section 3.7 is easy to obtain. The **form** of the solution for \vec{H} is independent of the applied load — only the magnitude depends on the load. Integrating the magnetic field as in Eq. 3.128 (and noting that the μ terms from Eq. 3.128 and Eqs. 3.124–3.125 cancel out):

$$\Phi_{z_{\text{in}}} = -2\pi(0.2286a^3\Theta) \quad (3.129)$$

$$\Phi_{z_{\text{out}}} = 0 \quad (3.130)$$

and similarly for the r component,

$$\Phi_{r_{\text{in}}} = -2\pi(1.595a^3\Theta) \quad (3.131)$$

$$\Phi_{r_{\text{out}}} = -2\pi(5.599a^3\Theta) \quad (3.132)$$

These solutions are proportional to $a^3\Theta$. From the definition of Θ , it is apparent that

$$a^3\Theta = \frac{1 - \nu^2}{E^*} e_{15} p_0 a^2 \quad (3.133)$$

The most interesting data to look at in the experiments will be the vertical flux Φ_z vs. either load P or displacement δ . It is apparent, then, that

$$\Phi_z = -1.436 \frac{1 - \nu^2}{E^*} \frac{3}{2\pi} e_{15} P \quad (3.134)$$

and, since $\delta = \left(\frac{9}{16} \frac{P^2}{RE^*x}\right)^{1/3}$,

$$\Phi_z = -1.436(1 - \nu^2) \frac{2}{\pi} \sqrt{R} e_{15} \delta^{3/2} \quad (3.135)$$

Most obviously, these equations are the functional dependence of the magnetic flux on applied load or on indentation depth. It is seen, however, that the flux as a function of depth does not depend on the Young's modulus of the material, or alternatively that the flux as a function of load does not depend on the radius of curvature of the indenter. This is understandable, given that this solution is for an incompressible material. Determining e_{15} , for example, would then be a simple matter of measuring the slope of a Φ - P curve.

From Berlincourt [19], we expect e_{15} to be on the order of $\frac{1}{2}e_{33}$. Values of e_{15} are therefore (see Table 4.1) on the order of 500 Tesla per unit strain. Applying this theory, which is only truly applicable in the case of an incompressible material, to the properties of Terfenol-D for a typical indentation test (where the composite radius of curvature $R \approx 1inch$ and the maximum load applied $P \approx 5N$) shows that the total flux change will be extremely small:

$$\Phi_z = -1.436 \cdot \frac{0.91}{40 \cdot 10^9 \text{ Pa}} \cdot \frac{3}{2\pi} \cdot 500 \text{ T} \cdot 5 \text{ N} \approx 4 \text{ Maxwells} = 4 \cdot 10^{-7} \text{ Webers} \quad (3.136)$$

This flux change is extremely small; it is near the limit of resolution for current commercial fluxmeters. Magnetic noise in the environment could drown out such a signal. An appropriately sized and placed gaussmeter, though, should be able to detect such a signal.

The solution for Φ_r suggests that the horizontal (r) flux will be much stronger. Unfortunately, mounting a horizontal pickup coil in the indenter is extremely impractical.

3.9 Outline of Other Solution Methods

The solution presented above is of course not unique in its methodology and assumptions. Solutions for other values of Poisson ratio can be evaluated. Solutions from the other representation (i.e., σ, H instead of σ, B) could also be studied. In addition, the solution above makes certain assumptions which may not be tenable for actual experiments. Namely, it assumes that the magnetostrictive constants are, in fact, constant as a function of magnetic field or stress state. This is known to not be true [1, 7]. Some aspects of the above limitations are discussed in this section.

3.9.1 Particular Solution: Isotropic, Compressible ($\nu = 0$) Solid; (σ, B) Representation

At the opposite end of the compressibility spectrum is the case of complete compressibility: $\nu = 0$.

$$E \left(\frac{\partial^2 u_r}{\partial r^2} + \frac{1}{r} \frac{\partial u_r}{\partial r} - \frac{u_r}{r^2} \right) + \frac{E}{2} \frac{\partial^2 u_r}{\partial z^2} + \frac{E}{2} \frac{\partial^2 u_z}{\partial r \partial z} - e_{15} \frac{\partial H_r}{\partial z} - e_{31} \frac{\partial H_z}{\partial r} = 0 \quad (3.137)$$

$$\frac{E}{2} \left(\frac{\partial^2 u_z}{\partial r^2} + \frac{1}{r} \frac{\partial u_z}{\partial r} \right) + E \frac{\partial^2 u_z}{\partial z^2} + \frac{E}{2} \frac{\partial}{\partial z} \left(\frac{\partial u_r}{\partial r} + \frac{u_r}{r} \right) - e_{15} \left(\frac{\partial H_r}{\partial r} + \frac{H_r}{r} \right) - e_{33} \frac{\partial H_z}{\partial z} = 0 \quad (3.138)$$

$$e_{15} \left(\frac{\partial^2 u_z}{\partial r^2} + \frac{1}{r} \frac{\partial u_z}{\partial r} \right) + e_{33} \frac{\partial^2 u_z}{\partial z^2} + (e_{15} + e_{31}) \frac{\partial}{\partial z} \left(\frac{\partial u_r}{\partial r} + \frac{u_r}{r} \right) + \mu_{11} \left(\frac{\partial H_r}{\partial r} + \frac{H_r}{r} + \frac{\partial H_z}{\partial z} \right) = 0 \quad (3.139)$$

This system of equations does not separate and simplify as much as in the incompressible case. By making some interesting coordinate changes, however, we can reduce the equations to a simpler, mostly decoupled set of equations. Specifically, we perform the three following transformations:

$$\left(\frac{\partial u_z}{\partial r} \right)' \rightarrow \frac{\partial u_z}{\partial r} - \frac{2e_{15}}{E} H_r \quad (3.140)$$

$$\left(\frac{\partial u_r}{\partial r} + \frac{u_r}{r} \right)' \rightarrow \frac{\partial u_r}{\partial r} + \frac{u_r}{r} - \frac{e_{31}}{E} H_z \quad (3.141)$$

$$z' \rightarrow -z/4 \quad (3.142)$$

with the aim of simplifying the PDEs. Using these transformations (and remembering that $e_{31} = -e_{33}/2$), Eqs. 3.137–3.139 then become

$$E \frac{\partial}{\partial r} \left(\frac{\partial u_r}{\partial r} + \frac{u_r}{r} \right)' + \frac{E}{2} \frac{\partial^2 u_r}{\partial z^2} + \frac{E}{2} \frac{\partial}{\partial z} \left(\frac{\partial u_z}{\partial r} \right)' = 0 \quad (3.143)$$

$$\frac{E}{2} \left(\frac{\partial}{\partial r} \left(\frac{\partial u_z}{\partial r} \right)' + \frac{1}{r} \left(\frac{\partial u_z}{\partial r} \right)' \right) + E \frac{\partial^2 u_z}{\partial z^2} + \frac{E}{2} \frac{\partial}{\partial z} \left(\frac{\partial u_r}{\partial r} + \frac{u_r}{r} \right)' - \frac{5}{4} \frac{\partial H_z}{\partial z} = 0 \quad (3.144)$$

$$e_{15} \left(\frac{\partial}{\partial r} \left(\frac{\partial u_z}{\partial r} \right)' + \frac{1}{r} \left(\frac{\partial u_z}{\partial r} \right)' \right) + e_{33} \frac{\partial^2 u_z}{\partial z^2} + (e_{15} + e_{31}) \frac{\partial}{\partial z} \left(\frac{\partial u_r}{\partial r} + \frac{u_r}{r} \right)' + \frac{2e_{15}^2}{E} \left(\frac{\partial H_r}{\partial r} + \frac{H_r}{r} \right) + (e_{15} + e_{31}) \frac{e_{31}}{E} \frac{\partial H_z}{\partial z} + \mu_{11} \left(\frac{\partial H_r}{\partial r} + \frac{H_r}{r} + \frac{\partial H_z}{\partial z} \right) = 0 \quad (3.145)$$

The second equation does not completely decouple the mechanical and magnetic behavior. (The $z' \rightarrow -z/4$ equation was not used above; if it were, then $dz' \rightarrow -4dz$, and the second equation would decouple, but the first equation would not.) The coupling of the material properties in Eq. 3.145, though, is interesting: there is a factor of $\frac{2e_{15}^2}{E} + \mu_{11}$ multiplying the H_r terms, and $(e_{15} + e_{31})\frac{e_{31}}{E} + \mu_{11}$ multiplying the H_z term.

3.9.2 Stress and Magnetic Field (σ , H) Representation

The following is an outline of an alternative solution method, using the PDEs derived in Section 3.5.2 as a starting point. It should be reiterated that this solution assumes $J_{\text{free}} = 0$.

3.9.2.1 Isotropic, Incompressible Material

By use of $\nu = 0.5$, the first two equations again decouple from the latter equations. But now, instead of a single equation with magnetic variables, there is a system of two equations.

$$h_{15} \frac{1}{r} \left(\frac{\partial^2 u_r}{\partial r \partial z} + \frac{\partial^2 u_z}{\partial r^2} \right) - \nu_{11} \frac{1}{r} \frac{\partial B_r}{\partial r} = 0 \quad (3.146)$$

$$-(h_{15} + h_{33}) \frac{\partial^2 u_z}{\partial r \partial z} + h_{31} \left(\frac{\partial^2 u_r}{\partial r^2} + \frac{1}{r} \frac{\partial u_r}{\partial r} - \frac{u_r}{r^2} \right) - h_{15} \frac{\partial^2 u_r}{\partial z^2} + \nu_{11} \left(\frac{\partial B_r}{\partial z} + \frac{\partial B_z}{\partial r} \right) = 0 \quad (3.147)$$

If we again use separation of variables, we have to go to the magnetic scalar potential anyway, because the PDEs involve both B_r and B_z . So, letting $\vec{B} = -\mu_{ij} \nabla \phi_M$,

$$-\frac{1}{r} \frac{\partial^2 \phi_M}{\partial r^2} = 0 \quad (3.148)$$

$$\frac{\partial^2 \phi_M}{\partial r \partial z} + \frac{\partial^2 \phi_M}{\partial z \partial r} = 0 \quad (3.149)$$

and if $\phi_M = R(r)Z(z)$, then

$$-\frac{1}{rR} \frac{\partial^2 R}{\partial r^2} = 0 \quad (3.150)$$

$$\frac{\partial R}{\partial r} \frac{\partial Z}{\partial z} + \frac{\partial R}{\partial r} \frac{\partial Z}{\partial z} = 0 \quad (3.151)$$

3.9.3 Magnetostrictive “Constants”

Recalling the definition of the d_{ij} from Eq. 1.10 and referring to Figure 1-2, it is apparent that the general functional behavior of d_{33} is as shown in Figure 3-6. We would expect similar behavior as a function of load, but no plots of B versus σ have been found in the literature to confirm this expectation.

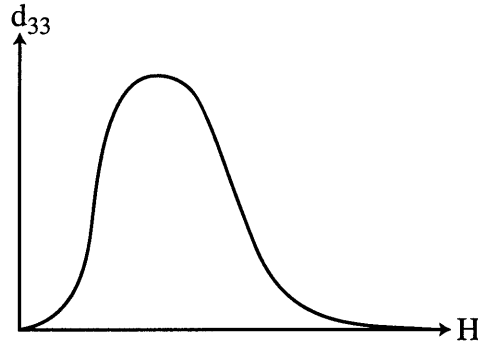


FIGURE 3-6: General functional behavior of d_{33} .

The maximum load applied in the experiments can be large enough to create a noticeable change in magnetization, limited only by the restriction that it not create any plastic deformation in the material (see Section 4.2.1.3). The maximum stress inside the specimen is, therefore, relatively large and it is not unreasonable to expect the magnetostrictive constants to change significantly. This effect could be accounted for by integrating d_{ij} over the changing stress. This would be straightforward in the context of a uniaxial test, as the total uniaxial strain would simply be the integral of the d_{33} over the magnetic field (alternatively, the total change in B_3 would be the integral of d_{33} over the change of σ_{33}). In fact, the calculated magnetization change versus load would depend on the original state (initial magnetic field and stress) of the specimen because the original state would define the lower bound of the integral (i.e., the start and end points of the integration would be different values of H in Figure 3-6 above). Extending this technique to the three-dimensional stress state characteristic of indentation, however, would be quite difficult.

Chapter 4

Experimental Design

Officer: *“It’s never been calibrated, you know.”*

Captain/Scientist: *“It’s a planet–destroying superlaser! We can turn that whole world into rubble. How well does it need to be calibrated?!?”*

—Kevin J. Anderson’s “Champions of the Force”

In addition to a theoretical framework for analyzing indentation of magnetostrictive materials, an experimental apparatus is required which can simultaneously measure mechanical data (e.g., load and displacement) and magnetic data (e.g., magnetic flux). No such apparatus is currently commercially available. This chapter presents a preliminary experimental design concept for such an apparatus.

An experimental apparatus can not be properly designed without some knowledge of the properties of the materials to be tested, and so the first section of this chapter presents and discusses relevant properties of some candidate materials. The second section details the design of the apparatus. Next is a suggested experimental procedure. Last is a discussion of the experimental indentation of magnetostrictive materials.

4.1 Material Properties

Properties of the materials chosen for study and their sources are shown in Tables 4.1 and 4.2. Note that the c_{ij} and e_{ij} data are generally for single crystals.

The values for e_{15} and e_{33} in Table 4.1, shown in parentheses, were calculated from other data [1,3,12, others] using Eq. 3.40. Question marks indicate that data could not be found in the literature. Elastic stiffness components were measured at zero magnetization.

	c_{11}	c_{12}	c_{44}	Max. e_{15}	Max. e_{33}	μ_{33}^R
Units	GPa			Tesla		μ_0
Pure Ni	250	160	118	?	(-704)	110 to 600 [20]
Pure Fe	241	146	112	?	?	150 to 5000 [20]
Tb _{0.3} Dy _{0.7} Fe _{1.9-2}	141 [3]	64.8 [3]	48.7 [3]	(~500 to 800)	(640) or (910)	5-10 3-4 [21] 1.8 [22] 10-15 [23]
Hiperco (2%-V Permendur)	?	?	?	(10 ⁴ [12])	(10 ⁴ – 10 ⁵ [12])	800 to 4500 [1]

TABLE 4.1: Tensor Property Values for Single Crystals

Iron and nickel were chosen because their magnetostrictive behavior has been extensively studied, and so results from indentation tests could be compared to data from the large body of literature. Terfenol was chosen because it is one of the most important magnetostrictive materials in use today. Finally, Hiperco-50 was chosen because of its near-zero anisotropy energy and its high yield strength (as mentioned before, it is necessary to avoid plastic deformation of the samples, and thus materials with higher yield strengths are preferred). The Poisson ratio of Hiperco-50 has not been reported to date, so the c_{ij} are not given in Table 4.1. Its Young's modulus is close to that of iron, so the components of the stiffness tensor are expected to be comparable. These components could be measured directly by spherical indentation.

4.2 Apparatus

4.2.1 Design

Combining mechanical indentation and magnetic field measurements leads to a set of competing requirements for and strong limitations on the experimental apparatus. In the most basic form of these experiments, spherical indentation is done while measuring the change in magnetic field near the indenter. Conceptually, the easiest way of doing this is to wind a wire around the indenter to form a pickup coil, as shown in Figure 4-1. In reality the apparatus is slightly more complicated.

Property	Units	Pure Ni	Pure Fe	Terfenol-D	Hiperco-50
Mechanical					
Density	g/cm ³	8.90	7.88	9.25	8.12
Young's Modulus	GPa	207	200	44 @ 0 Oe [3] 106 @ 4 kOe [3] $E^H = 29-40$ [21] $E^H = 45-55$ [24] $E^B = 15-25$ [24] $E = 40$ [25] $E = 30$ [26]	207
Poisson's Ratio ν	—	0.31	0.29	0.4 [25]	?
Yield (Rupture) Strength	MPa	138	130	700 compression [27] 28 tension [27]	300-400
Vickers Hardness	GPa	0.7-1.0	2.44	6.06 [28]	?
Magnetic					
T_{Curie}	Kelvin	631	1043	653	1213
$M_{\text{saturation}}$	Tesla	0.63	2.16	1.0 [29]	2.2
Magnetoelastic					
d_{33}^{max} (for various values of pre-stress and offset magnetic field)	nm/A	-3.1	?	9-25 [13] 5-11 [21] 17-23 [23] 10-15 [30] 40-45 [31] 8.5 [32] 30-50 [33] 25-200 [34]	38?
$\lambda_{\text{saturation}}$	—	10^{-5}	10^{-5}	10^{-3}	$60 \cdot 10^{-6}$

TABLE 4.2: Miscellaneous Material Property Data

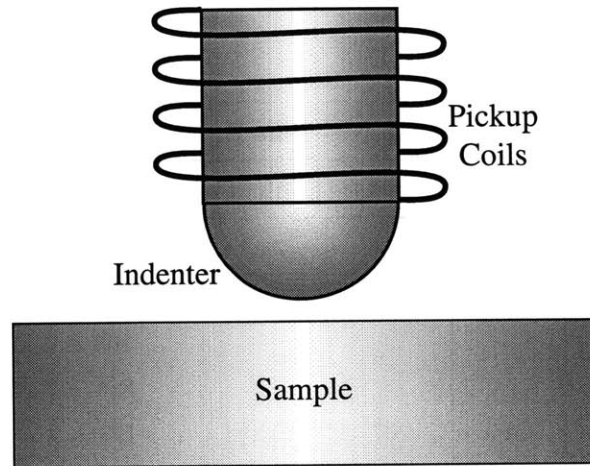


FIGURE 4-1: A diagram of a basic indenter/pickup coil arrangement.

A pickup coil detects flux ($\Phi = \vec{B} \cdot \vec{A}$) by integrating a changing voltage ($V = -N\partial\Phi/\partial t$, where N is the number of turns of wire; N should be maximized to create as large a voltage signal as possible). Ideally, the pickup coil would be of approximately the same diameter as the generated field in order to measure the entire field, but this can not happen for two reasons. First, the diameter of the generated field is too small. Consider the size of the indenter contact radius to see why this is so. The contact radius $a = (3PR/4E^*)^{1/3}$ is at most $200 \mu\text{m}$ in our experiments, and theory (See Chapter 3) predicts that most of the change in magnetic field will be inside the contact area, so the major change in field will occur inside an area with a diameter less than 0.5 mm . Wrapping wires around a post with a diameter less than 0.5 mm is impractical. Second, the mechanics of indentation requires that the indenter should be at least 10 times the size of the contact area [35]. This requirement alone already forces a ratio of total pickup coil area to the signal area of 100:1, which has implications for the amount of noise and drift in the flux signal.

An indenter/pickup coil design has been completed; a diagram is shown in Figure 4-2. An Instron 4505 screw-driven tensile testing machine has been modified for these experiments. The indenter is mounted on the fixed crosshead. The sample is mounted on the mobile crosshead. A magnetic pickup coil is also mounted on the indenter and is centered on the sample. A 50 lbs. load cell is mounted above the indenter to accurately measure the applied load, and a photonic sensor (see Section 4.2.1.4) is mounted near the indenter to accurately measure displacement. The load cell, photonic sensor, and the pickup coil are connected to a National Instruments data acquisition card on a PC; LabView reads in, plots, and saves the data.

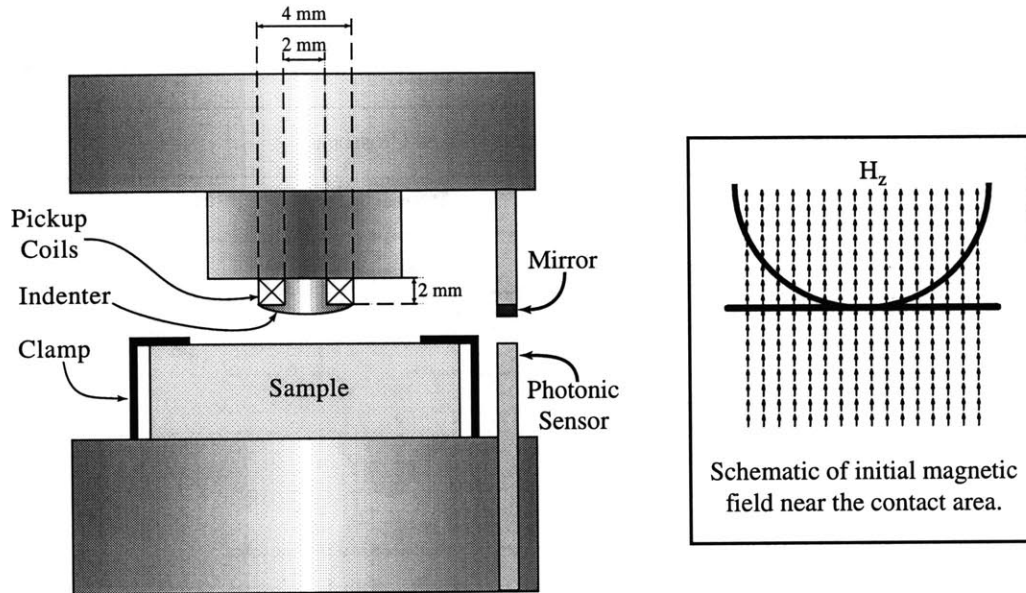


FIGURE 4-2: Close-in view of the indenter arrangement.

Note that the clamps are very important for the unloading portion of microindentation¹ [36]. Adhesion can be significant at the loads and displacements encountered in these experiments, and a secure clamp on the sample is necessary to ensure an accurate unloading curve. Given that the samples are ferromagnetic, the clamping will also be necessary to secure the samples in place.

4.2.1.1 Solenoid Design

The “linear” magnetoelastic response of magnetostrictive materials depends on the magnetization of the material, and therefore we must be able to apply a variable magnetic field to our sample. The best way to do this is to enclose the indenter in a solenoid, as shown in Figure 4-3. Note that, because of space restrictions inside the solenoid, the mirror is extended down on an aluminum rod (which slides freely in a groove in the side of the main column) to a space below the solenoid, where there is room for the micrometer stage-mounted photonic sensor. Also note the complete use of non-magnetic materials near the indenter except for the iron yoke to avoid affecting the fields. The solenoid would consist of copper wires wrapped tightly around a DelronTM tube. The inner diameter of the solenoid would

¹“Microindentation” refers to instrumented indentation at a load on the order of a few grams; it generally means that the indentation depth is on the order of micrometers. One important characteristic is that it uses an independent displacement sensor. We implement this via a photonic position sensor which uses the intensity of light reflected off a mirror to measure distance.

be 5.1 cm, the outer diameter of the windings would be 12 cm, and the length would be 25 cm. See Montgomery [37] for details of solenoid design.

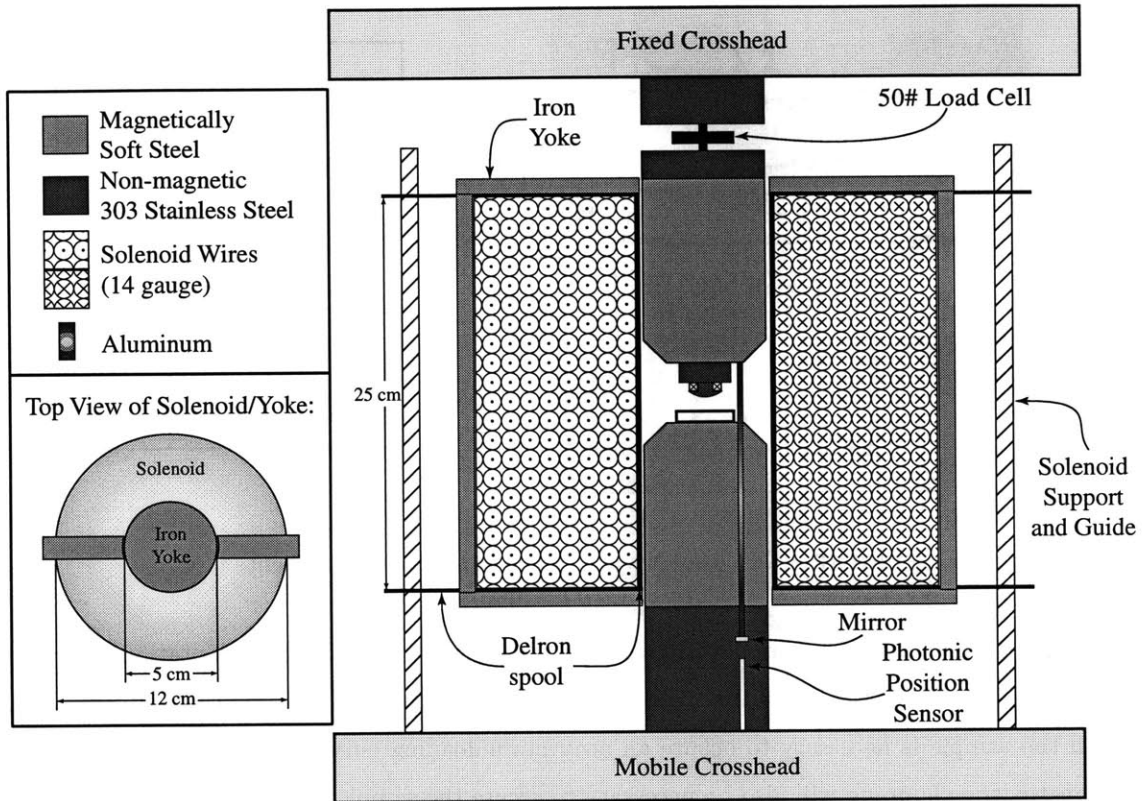


FIGURE 4-3: Cross-sectional view of the indenter, solenoid, and iron yoke. The inset figure shows the top view of the iron yoke and the solenoid.

Part of the solenoid design process is to determine the maximum required field strength. This is controlled by two factors: the magnetic field required for saturation in an ideal case, and the demagnetization factor. Remember that the permeability of a material is related to the susceptibility: $\mu = \mu_0(1 + \chi)$. A given sample geometry has an effective susceptibility, given by the following relation:

$$\chi_{eff} = \frac{\chi}{1 + n\chi} \quad (4.1)$$

where n is the demagnetization factor described in Section 1.1. $n \rightarrow 0$ as a rod becomes infinitely long, and $n \rightarrow 1$ as the rod becomes infinitesimally short. The samples used are disks on the order of 2.5 cm in diameter and 1 mm to 7 mm thick, and so the demag factor n is greater than 0.5. For this case, then, $\chi \approx 500$ gives $\chi_{eff} \approx 2$. The resulting low value for the relative permeability means that the desired field strength in the material must be created almost exclusively with the solenoid.

Ideally, an extremely long solenoid with a variable power supply would provide a variable magnetic field strength. Size and power limitations along with the sample demagnetization factor, however, require an iron yoke to augment the solenoid's applied field (which can only achieve about 485 Gauss). The large bore size required to fit the indenter and sample is one factor limiting the maximum field strength; heat generation is another factor. Iron is very soft, however, and is therefore easily saturated with a small field. It has a saturation magnetization of about 2.2 Tesla.

The ideal magnetization curve (for a ring of material, i.e., a closed circuit, or an infinitely long rod) of a soft magnetic material, as shown in Figure 4-4, has a discontinuity between $+M_s$ and $-M_s$ at $H = 0$ (i.e., $\mu = \infty$). A gap in this circuit shears the curve over, giving it a finite slope. By choosing this gap size properly, we can control the range of magnetization available and thereby provide control over the strength of the field in the gap by changing the applied field from the solenoid.

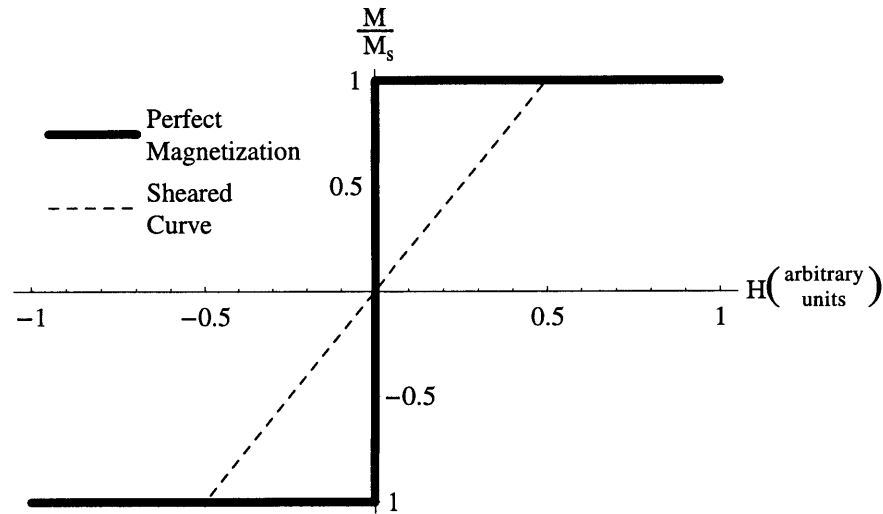


FIGURE 4-4: Perfect and sheared magnetization curves, in arbitrary units.

Design of the solenoid and iron yoke is done using linear magnetic circuit theory. The sum of all electromotive forces (EMF) and resistive drops in a magnetic circuit equals zero:

$$\sum NI - \sum R_m \Phi = 0 \quad (4.2)$$

where NI , the current-turns (i.e., the current times the number of windings), is for any type of EMF (e.g., solenoids, permanent magnets), and R_m is the reluctance. The reluctance of a section is equal to its length divided by the product of its permeability and cross-sectional area: $R_m = l/(\mu A_{cs})$. Because the permeability of iron is so much higher than air, the assumption that all magnetic flux is confined to the iron yoke is a reasonable one. Assuming a yoke thickness of about 2 cm, a solenoid length of

about 25 cm, a yoke bore diameter of 5 cm, and a gap height of about 2.5 cm, then the iron reluctance (which is on the order of $2 \cdot 10^5$ A/T m²) is a tiny fraction of the gap reluctance (which is on the order of 10^7 A/T m²). Assuming a magnetic field density in the air gap of 4000 Gauss, the electromotive force required from the solenoid is about 11,700 Amp–turns. For a solenoid with an inner diameter of 5 cm and an outer diameter of 12 cm, using 14 gauge wire, this translates into about 110 W of power required (4 Amps at 28 Volts); the temperature change of the solenoid due to resistive wire heating after 10 minutes is expected to be less than 8°C.

Note that, as shown in Figure 4-3, all pieces of the indenter and load train except for the solenoid yoke are made of non-magnetic 303 stainless steel. The iron yoke is made of a magnetically soft cold-rolled steel.

4.2.1.2 Pickup Coil and Fluxmeter Considerations

The sensitivity of a pickup coil is proportional to the number of turns N in the coil (remember $V = -N\partial\Phi/\partial t$). Most fluxmeters report units of Maxwell–turns. That is, the actual number of Maxwells measured is the reported number of Maxwell–turns divided by the number of turns in the pickup coil.

Most fluxmeters have a minimum range of 1000 Maxwell–turns. A coil with 150 turns would therefore in theory be able to report down to a range of about 6.7 Maxwells (equivalent to, for a pickup coil of the same diameter as mine but with a uniform magnetic field, a field density of 213 Gauss). LakeShore Cryotronics fluxmeter model 410 uses Volt–seconds as the basic unit of measurement. It has a minimum range of 3 mV–s, which is equal to 300,000 Maxwell–turns. The sensitivity is $5 \mu\text{V-s}$, which is equivalent to $5 \cdot 10^{-7}$ Webers (50 Maxwells).

Even if indentation were to cause an extremely large change in field density (as high as, say, M_s), the total flux change would be small because the change would occur only over a small area. Consider:

$$\Phi = BA_{\text{contact}} = (1 \text{ T}) (\pi \cdot 150 \cdot 10^{-6} \text{ m})^2 \approx 10^{-7} \text{ Webers} = 10 \text{ Maxwells} \quad (4.3)$$

So it becomes clear that measurement of the magnetic field will be difficult.

In a 2 mm x 2 mm cross section, using 38 gauge wire (the thinnest which could easily be acquired and wound), a maximum of about 250 turns could in theory be wound. In practice, we were able to wind 110 ± 10 turns.

4.2.1.3 Indenter Design

There are three conditions which govern the radius of curvature of the indenter head. The most important one is that the sample be at least 10 times as thick as the contact radius, in order to ensure

that classical indentation results (which assume an infinite half-space) still apply. The next most important condition is that the material not be plastically deformed, so that the magnetic state of the body does not permanently change. The final condition is that the depth of indentation be large enough that noise from the indenter machine and imperfections in the spherical nature of the indenter do not overwhelm the signal. Mathematically, these three conditions are:

$$a \leq 0.1t \quad \rightarrow \quad R \leq 0.00133 \frac{E^* t^3}{P} \quad (4.4)$$

$$p_{max} \leq 1.1\sigma_{yield} \quad \rightarrow \quad R \geq 0.3813 \frac{E^* \sqrt{P}}{\sigma_{yield}^{3/2}} \quad (4.5)$$

$$\delta \geq h_{min} \quad \rightarrow \quad R \leq \frac{9}{16} \frac{P^2}{E^* h^3} \quad (4.6)$$

Figure 4-5 plots these three conditions for Terfenol-D, assuming a composite modulus² of 40 GPa, a maximum depth of indentation of 1.5 μm , a sample thickness of 2.4 mm, and a yield strength of 250 MPa. (This is the limiting yield strength of the steel indenter; Terfenol has a higher compressive rupture strength.)

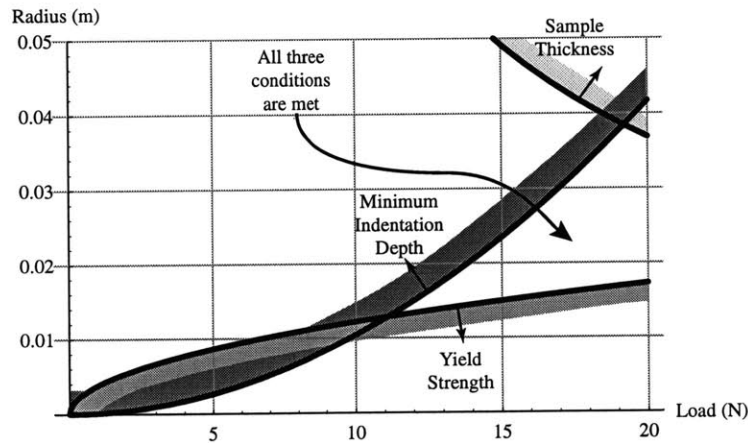


FIGURE 4-5: Design of the indenter head for use with Terfenol-D. Each line indicates the border of one design condition, and the shading and arrow indicates in which direction the condition is violated. The triangular area is where all three are met simultaneously (i.e., on the opposite side of the shading for all three lines).

Figure 4-6 plots the three conditions for Hiperco-50, assuming a composite modulus of 110 GPa, a maximum depth of indentation of 0.5 μm , a sample thickness of 1.5 mm, and a yield strength of 250

²See Appendix A for a definition.

MPa. (This is a slightly conservative estimate for the yield strength; the exact yield strength for my sample is not known, but is estimated to be anywhere from 200 to 400 MPa.)

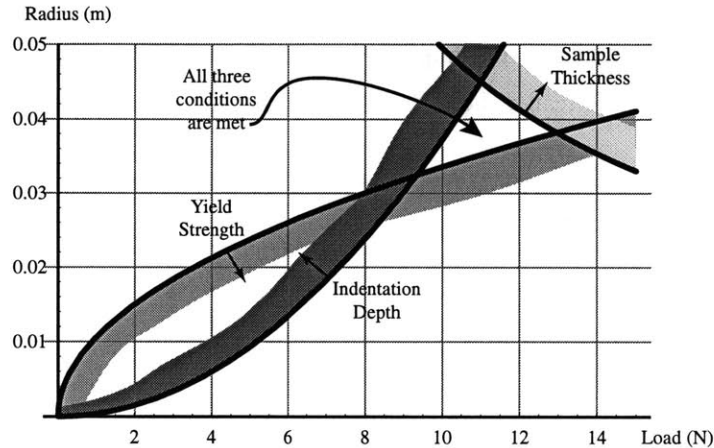


FIGURE 4-6: Design of the indenter head for use with Hiperco-50. Each line indicates one condition, and the shading and arrow indicates in which direction the condition is violated. The small triangular area is where all three conditions are met simultaneously.

4.2.1.4 Displacement and Load Measurement

Instrumented microindentation requires a system of displacement measurement which is independent of the indenter's mechanisms (i.e., which accurately reports the displacement of the indenter head, and not some point away from and under compression with the indenter head) [36].

Displacement is measured using an MTI 2000 Fotonic Sensor, which reflects light off of the mirror shown in Figures 4-2 and 4-3. This optic sensor has a resolution of about $0.01 \mu\text{m}$. Load is measured using a SensotecTM 50 lb. load cell. The resolution of this load cell is about 0.01 N; experimental noise limits its precision to about 0.1 N.

4.2.1.5 Permanent Magnets

Before expending the time, money and effort to construct a powerful solenoid, tests were conducted using small permanent magnets to create a local field, by placing them underneath the sample. Two types of round permanent magnets (with the magnetization direction perpendicular to the plane of the circle) were purchased from Dexter Corporation, Billerica, MA. The magnetically weaker ones were made of

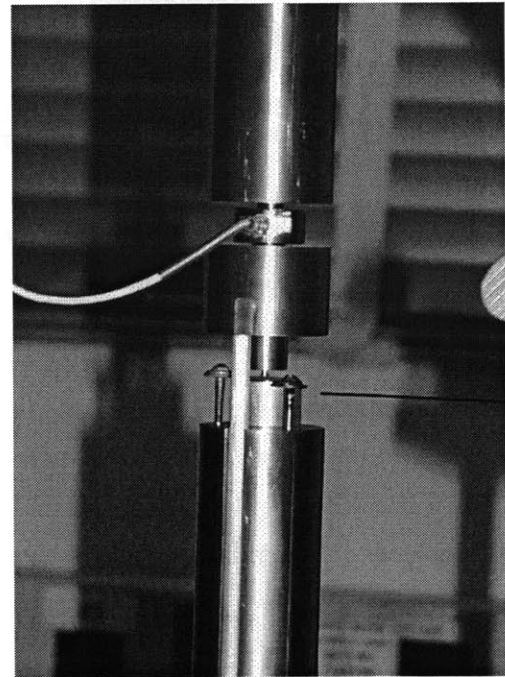
Ferrite, with a diameter of 1.18 inches, a thickness of 0.524 inches, and a remanent magnetization of 3,850 Gauss. The other ones were made of AlNiCo, with a 1.00 inch diameter, 0.375 inch thickness, and a remanent magnetization of 8,200 Gauss.

4.2.1.6 Construction

Construction of the experimental setup described above has begun. It is shown in Figure 4-7. The Instron 4505 machine itself is made of ferromagnetic materials, but these are far away from the indenter head and specimen, and thus do not significantly affect the magnetic field there. Calibration and testing using this setup is being performed.



(a) Indenter setup



(b) Zoom of indenter and specimen

FIGURE 4-7: Photo of experimental setup

4.2.2 Improved Designs

Hall probe gaussmeters provide much more accurate and sensitive measurements of magnetic field than pickup coils. These gaussmeters utilize the Hall effect to measure fields down to the milligauss range. On first inspection, it would seem that a Hall probe could not get close enough to the indentation area to provide a representative signal (see Section 4.2.1.2). By integrating the Hall probe “slab” with an indenter, however, the probe can be centered on the indenter and brought close to the indentation. The probe would have to be made of a material which has either zero or a known response to stress, and the effective modulus of the “composite” indenter would need to be properly accounted for. Figure 4-8 diagrams the geometry of such a gaussmeter/indenter system.

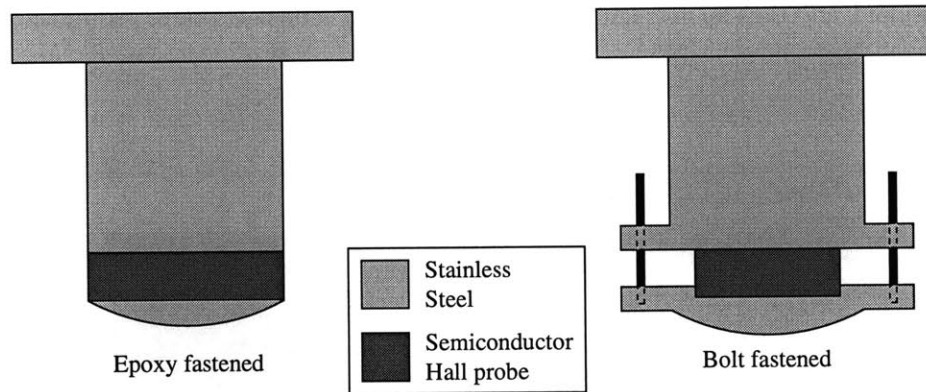


FIGURE 4-8: Two designs for a Hall probe-based magnetic indenter. The electrical leads to the Hall probe are not shown.

A more challenging design would involve making the indenter head itself out of a semiconductor, thus allowing measurement of the magnetic field directly at the contact area. Another, more complicated possibility is to use giant magnetoresistive (GMR) films. As the name implies, the resistance of GMR films changes drastically with changes in the magnetic field. A GMR thin film could be deposited on the indenter and its resistive response calibrated with a locally applied field.

4.3 Experimental Procedure

1. Horizontally position the sample underneath the indenter
2. Raise lower crosshead with manual controls so that sample and crosshead are close (preferably within $50\ \mu\text{m}$), but not touching (use visual inspection to ensure separation of surfaces)

3. Bring lower crosshead higher (but not in contact) with fine controls set at 10 – 20 $\mu\text{m}/\text{minute}$, in order to give the tensile testing machine a baseline from which to improve its speed control³.
4. Set experiment indent speed, and change any necessary parameters in the data acquisition program (e.g., data acquisition rate).
5. Calibrate photonic sensor if the lower crosshead has been moved more than 1 mm away from the indenter head since the last calibration.
6. Apply the magnetic field if the solenoid is being used:
 - (a) Raise the solenoid into position, vertically centered on the sample.
 - (b) Slowly apply power to the solenoid until the desired field strength is attained.
7. Start the data acquisition program averaging the signal from the load cell.
8. Once LabView has finished zeroing the load, start the lower crosshead moving up.
9. Stop the crosshead motion once the load is about 1 Newton below the maximum desired load (due to the delayed response of the tensile testing machine), then reverse the direction of the crosshead.
10. Once unloading is complete and the indenter has moved a few microns away from the surface, stop the data acquisition program recording and reset it in preparation for the next run.

³At the low speeds used for these indentations, the tensile testing machine (which has a minimum speed of 1 $\mu\text{m}/\text{min}$) can not immediately move at the exact set speed; it moves at a slower speed, gets a baseline from which to determine its real speed, then corrects the speed based on that. If it has just moved at a similar speed (e.g., 10 $\mu\text{m}/\text{min}$ instead of 5 $\mu\text{m}/\text{min}$) in the same direction, then it can accurately produce the new set speed without requiring a new baseline.

Chapter 5

Conclusions and Recommendations

So many worlds, so much to do,

So little done, such things to be.

—Alfred, Lord Tennyson

5.1 Conclusions

Indentation of magnetostrictive materials has the potential to be of use in a number of fields, most notably in the tribology of computer hard disks. Both a theoretical framework and an experimental design are required to fulfill that potential.

A theoretical framework for the analysis of indentation of magnetostrictive materials was presented. This framework allows the solving of the forward problem, that is, the prediction of specimen response given the material properties. Further, the reverse problem can be solved using the same framework, that is, extraction of material properties from the measurement of appropriate data during an indentation test.

This framework is based on a linear model of material response as presented in IEEE Standard 319. A set of three partial differential equations governing magnetostrictive behavior was presented. Next, these equations were solved for the case of an incompressible material. This limiting case (for which Poisson's ratio $\nu = 0.5$) provides many useful results. First, a closed form relation between the magnetic flux produced by an applied load was derived. The flux is seen to be directly proportional to the load, and the constant of proportionality includes the magnetostrictive constant e_{15} . Therefore, a Φ - P curve could be measured experimentally, and e_{15} could be determined from the slope of the curve. Alternately,

predictions of the magnetostrictive response for particular material conditions can be made. Second, the magnitude of the flux change is predicted to be extremely small. As mentioned in Chapter 1, a fully coupled theory of indentation of magnetoelastic materials has not heretofore been published. Much work remains to be done in refining the theory presented above, but the results derived in this thesis constitute an important step in the direction of a fundamental understanding of the indentation of magnetoelastic materials.

A preliminary experimental design for the indentation of magnetostrictive materials was then presented. This design incorporates the many competing design requirements of a mechanical indenter and a magnetic measurement system and solenoid. It would allow quantitative measurement of the vertical component of the magnetic flux just above the indenter contact area.

5.2 Future Work

5.2.1 Theory

The analytical solution presented in Chapter 3 is valid at the material surface, i.e., for $z = 0$. Solutions throughout the specimen could be obtained by solving for the classical mechanical displacements under an indenter, and substituting these displacements in for the non-homogeneous component of the partial differential equation that describes the coupling effect.

More general analytical solutions should also be developed. The case of a general value of Poisson ratio in the linear material model will be much more difficult than the incompressible case, because the three partial differential equations will not decouple.

A material model more appropriate to the experimentally observed material response should be developed. Magnetostrain has been observed to depend approximately quadratically on specimen magnetization. A nonlinear model which has such a quadratic behavior has been proposed, and is discussed briefly below.

5.2.1.1 Nonlinear Material Model

Carman and Mitrovic [13,14] derive the constitutive equations for a nonlinear magnetostrictive material response. The motivation for doing this is that the magnetostrain is, in fact, an even function of the magnetization. Their results, ignoring thermal coupling, are presented below. Beginning with a thermodynamical derivation, they arrive at a definition of the energy differential

$$dU = \sigma_{ij}d\varepsilon_{ij} + H_m dB_m + TdS \quad (5.1)$$

This is then used to create a Helmholtz free energy, which is then expanded in a Taylor series about an initial energy and terms which are not seen experimentally (e.g., linear terms) are discarded. Finally, they present constitutive laws in the (σ, B) representation:

$$B_m = H_n \mu_{mn}^\epsilon + \epsilon_{ij} H_n g_{ijnm} + \left\{ \frac{1}{2} \epsilon_{ij} \epsilon_{kl} H_n Q_{ijklnm} \right\} \quad (5.2)$$

$$\sigma_{ij} = \epsilon_{kl} C_{ijkl}^H - \frac{1}{2} H_n H_m g_{ijnm} - \left\{ \frac{1}{2} H_n H_m \epsilon_{kl} Q_{ijklnm} \right\} \quad (5.3)$$

where μ is magnetic permeability tensor, g is the new magnetostrictive tensor, Q is a higher order coupled stiffness tensor, and superscripts indicate variables held constant. The terms in braces are higher order terms which could be included, but may not be required. More detailed knowledge of the functional dependence of magnetostriction will indicate whether or not the term is required. Note that the product $H_m g_{ijnm}$ in the second equation could be interpreted as the e_{ijk} used in the linear model.

This nonlinear model could be used as the constitutive model for a numerical solution of the equilibrium equations presented in Chapter 3.

5.2.2 Experiments

Given the design considerations presented in Section 4.2.1, an indenter with a much smaller load and displacement range should be used in order to obtain more accurate data as well as greater control over the indentation depth. In addition to the experiments described in Chapter 4, there are numerous other related projects to be done. These include experimental investigations into the decay of magnetization due to elevated temperatures and indentation using a ferromagnetic indenter.

Sridhar et al [6] accurately measured the activation energy for decay of polarization in a piezoelectric material by repeatedly performing an indentation test, heating the material for some interval, then indenting again. The magnitude of the spontaneous magnetization decreases with temperature until, above the Curie temperature, magnets lose all spontaneous magnetization. Furthermore, there is a time-dependent decay of magnetization at elevated temperatures for some magnets. There are numerous differences in the polarization/magnetization behavior between piezoelectrics and magnetostrictives, but indentation does provide the potential for a simple tool for investigating magnetization decay in hard magnets.

The theory derived in Chapter 3 assumed a non-ferromagnetic indenter. Interesting results are expected for the case of a ferromagnetic indenter. This is expected due to the fact that the magnetic field is nearly perpendicular in air just outside a ferromagnetic material. Experiments using a ferromagnetic indenter should be conducted in order to further investigate this response.

Appendix A

Classical Indentation Results

This appendix presents a brief summary of the classical results of elastic indentation of two spheres [8].

A.1 Geometry

Figure A-1 shows the coordinate system and labels the bodies and their properties for indentation.

The composite modulus of the system is defined as

$$E^* \equiv \left(\frac{1 - \nu_1^2}{E_1} + \frac{1 - \nu_2^2}{E_2} \right)^{-1} \quad (\text{A.1})$$

and the “composite” radius of curvature (where both spherical surfaces are convex with respect to each other) is

$$R \equiv \left(\frac{1}{R_1} + \frac{1}{R_2} \right)^{-1} \quad (\text{A.2})$$

All my samples will be polished flat, and so $R_2 \rightarrow \infty$. Then $R \rightarrow R_1$.

A.2 General Values

For a circular point contact, the radius of the contact circle for a load P is:

$$a = \left(\frac{3PR}{4E^*} \right)^{\frac{1}{3}} \quad (\text{A.3})$$

The maximum contact pressure is

$$p_0 = \left(\frac{3P}{2\pi a^2} \right) = \left(\frac{6PE^{*2}}{\pi^3 R^2} \right)^{\frac{1}{3}} \quad (\text{A.4})$$

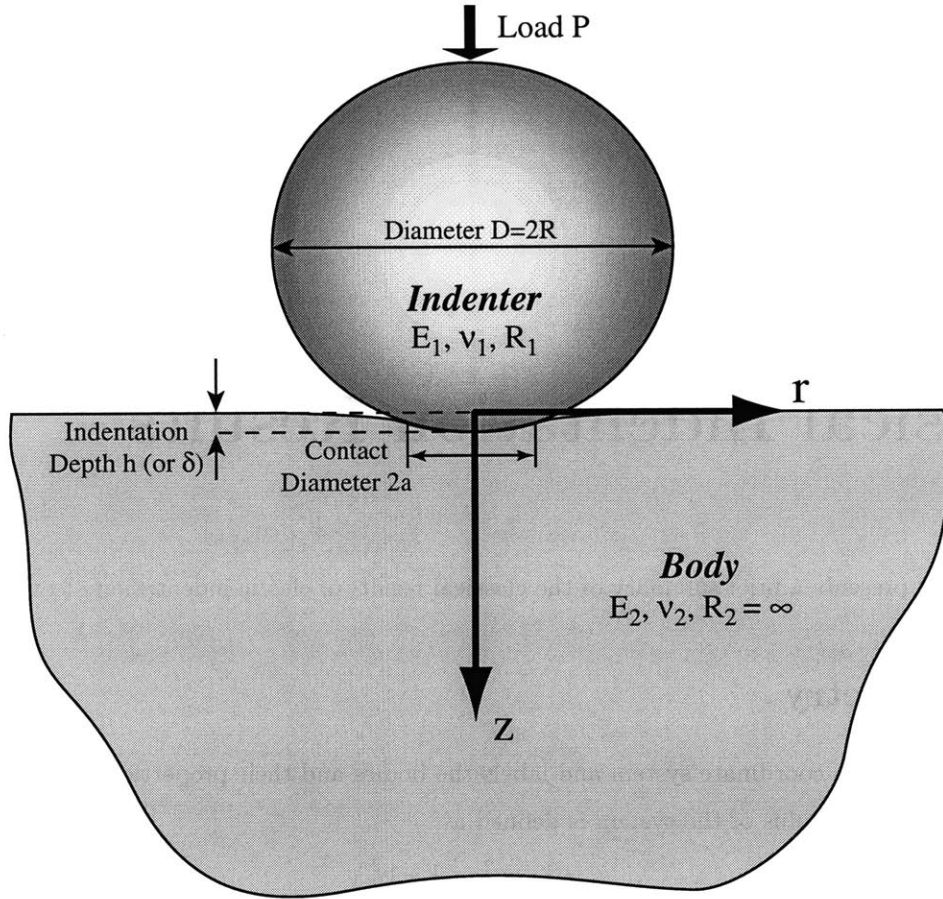


FIGURE A-1: Coordinate system and property values for indentation

And the separation between distant points is

$$\delta = \frac{a^2}{R} = \left(\frac{9}{16} \frac{P^2}{RE^{*2}} \right)^{\frac{1}{3}} \quad (\text{A.5})$$

The maximum shear stress is $\tau_1 = 0.31p_0$ at $r = 0, z = 0.48a$. The maximum tensile stress is $\sigma_r = \frac{1}{3}(1 - 2\nu)p_0$ at $r = a, z = 0$.

A.3 Displacements and Stresses

The equations for the displacements are as follows.

$$u_r(r, z = 0) = -\frac{(1 - 2\nu)(1 + \nu)}{3E} \frac{a^2}{r} p_0 \left(1 - \left(1 - \frac{r^2}{a^2} \right)^{\frac{3}{2}} \right) \quad r \leq a \quad (\text{A.6})$$

$$u_r(r, z = 0) = -\frac{(1 - 2\nu)(1 + \nu)}{3E} \frac{a^2}{r} p_0 \quad r > a \quad (\text{A.7})$$

$$u_z(r, z = 0) = \frac{1 - \nu^2}{E} \frac{\pi p_0}{4a} (2a^2 - r^2) \quad r \leq a \quad (\text{A.8})$$

$$u_z(r, z = 0) = \frac{1 - \nu^2}{E} \frac{p_0}{2a} \left((2a^2 - r^2) \arcsin(a/r) + r^2(a/r) \left(1 - \frac{a^2}{r^2} \right)^{\frac{1}{2}} \right) \quad r > a \quad (\text{A.9})$$

The stresses are as follows. On the surface, inside the loaded circle,

$$\sigma_r/p_0 = \frac{1 - 2\nu}{3} \left(\frac{a^2}{r^2} \right) \left\{ 1 - \left(1 - \frac{r^2}{a^2} \right)^{3/2} \right\} - \left(1 - \frac{r^2}{a^2} \right)^{1/2} \quad (\text{A.10})$$

$$\sigma_\theta/p_0 = -\frac{1 - 2\nu}{3} \left(\frac{a^2}{r^2} \right) \left\{ 1 - \left(1 - \frac{r^2}{a^2} \right)^{3/2} \right\} - 2\nu \left(1 - \frac{r^2}{a^2} \right)^{1/2} \quad (\text{A.11})$$

$$\sigma_z/p_0 = -\left(1 - \frac{r^2}{a^2} \right)^{1/2} \quad (\text{A.12})$$

And on the surface outside the loaded circle,

$$\sigma_r/p_0 = \sigma_\theta/p_0 = (1 - 2\nu) \frac{a^2}{3r^2} \quad (\text{A.13})$$

and of course $\sigma_z = 0$. Along the z axis within the solid, the stresses are

$$\sigma_r/p_0 = \sigma_\theta/p_0 = -(1 + \nu) \left\{ 1 - \frac{z}{a} \arctan(a/z) \right\} + \frac{1}{2} \left(1 + \frac{z^2}{a^2} \right)^{-1} \quad (\text{A.14})$$

$$\sigma_z/p_0 = -\left(1 + \frac{z^2}{a^2} \right)^{-1} \quad (\text{A.15})$$

Figures A-2 and A-3 below show the u_r and u_z functions at $z = 0$. Figure A-4 shows the stress components at $z = 0$.

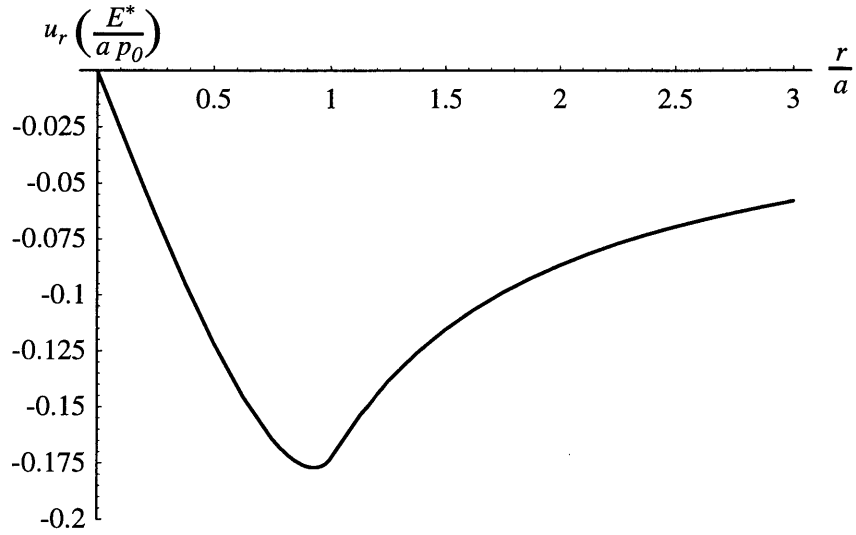


FIGURE A-2: u_r vs. r at $z = 0$ under a spherical indenter, assuming $\nu = 0.3$. Note the scale on the vertical axis ($u_r E^*/p_0 a$, which is on the order of 10^{-7} microns).

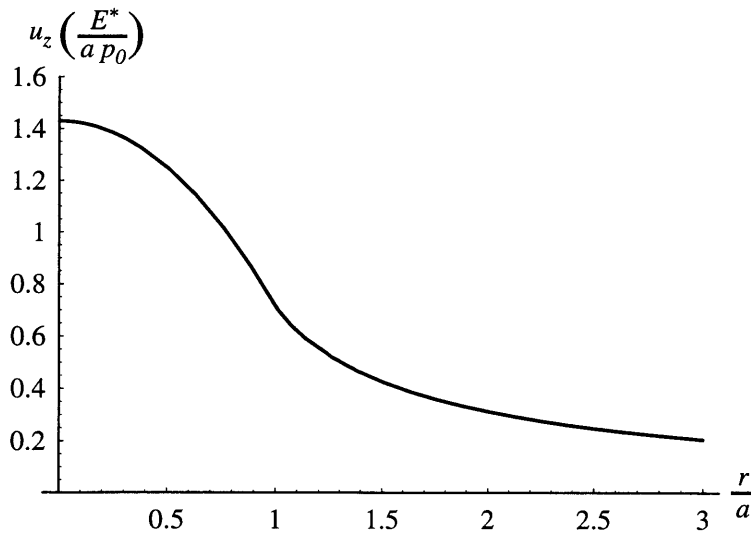


FIGURE A-3: u_z vs. r at $z = 0$ under a spherical indenter, assuming $\nu = 0.3$. Note the scale on the vertical axis ($u_r E^*/p_0 a$, which is on the order of 10^{-7} microns).

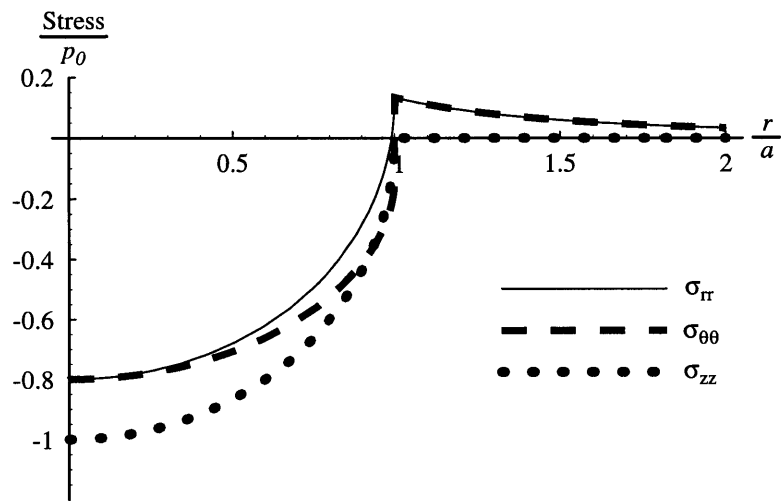


FIGURE A-4: Stresses vs. r/a at $z = 0$ under a spherical indenter, assuming $\nu = 0.3$. Note the scale on the vertical axis (σ/p_0).

Appendix B

Unit Conversions

Given the numerous unit systems used in magnetics as well as mechanics, the following unit conversions were found to be useful:

$$\begin{aligned}1 \text{ dyne/cm}^2 &= 10^{-1} \text{ Pa} \\1 \text{ Oe} &= 79.577 \text{ A/m} \\1 \text{ Henry} &= 1 \text{ kg m}^2 / \text{C}^2 \\1 \text{ Maxwell} &= 10^{-8} \text{ Weber} \\1 \text{ Tesla} &= 10^4 \text{ Gauss} \\&= 1 \text{ Weber/m}^2 \\1 \text{ Volt-second} &= 1 \text{ Weber} \\1 \text{ psi} &= 6894.8 \text{ Pa} \\1 \text{ Tesla} &= 1 \text{ Weber/m}^2 \\&= 1 \text{ N/A} \cdot \text{m} \\1 \text{ m/A} &= 1 \text{ Tesla/Pa}\end{aligned}$$

Bibliography

- [1] E. du T. de Lacheisserie, *Magnetostriction: Theory and Applications of Magnetoelasticity*. CRC Press, 1993.
- [2] J. D. Livingston, *Driving Force : The Natural Magic of Magnets*. Harvard University Press, 1996.
- [3] A. E. Clark, *Magnetostrictive Rare Earth-Fe₂ Compounds*, pp. 531–89. Ferromagnetic Materials, North-Holland Publishing Company, 1980.
- [4] A. E. Giannakopoulos and S. Suresh, “Theory of Indentation of Piezoelectric Materials,” *Acta Materialia*, vol. 47, no. 7, pp. 2153–64, 1999.
- [5] U. Ramamurty, A. E. Giannakopoulos, S. Suresh, and S. Sridhar, “An Experimental Study of Spherical Indentation on Piezoelectric Materials,” *Acta Materialia*, vol. 47, no. 8, pp. 2417–30, 1999.
- [6] S. Sridhar, A. E. Giannakopoulos, S. Suresh, and U. Ramamurty, “Electrical Response During Indentation of Piezoelectric Materials: New Method for Material Characterization,” *Journal of Applied Physics*, vol. 85, no. 1, pp. 380–7, 1999.
- [7] IEEE Standards Committee, “IEEE Standard on Magnetostrictive Materials: Piezomagnetic Nomenclature,” Standard 319, IEEE Ultrasonics, Ferroelectrics, and Frequency Control Society, 1990.
- [8] K. L. Johnson, *Contact Mechanics*. Cambridge University Press, 1985.
- [9] G. Hamilton, “Explicit Equations for the Stresses Beneath a Sliding Spherical Contact,” *Proceedings of Institution of Mechanical Engineers*, vol. 197C, pp. 53–9, 1983.
- [10] B. Bhushan, *Tribology and Mechanics of Magnetic Storage Devices*. Springer-Verlag, 1990.

- [11] W. Brown, *Magnetoelastic Interactions*. Springer-Verlag, 1966.
- [12] S. Zhakov, V. Borodin, and V. Ostanin, "Investigation of the Twist Deformation of Ferromagnetic Rods (Wiedemann Effect). II. Theory," *Fizika Metallov i Metallovedenie*, vol. 57, no. 1, pp. 45–51, 1984.
- [13] G. P. Carman and M. Mitrovic, "Nonlinear Constitutive Relations for Magnetostrictive Materials with Applications to 1-D Problems," *Journal of Intelligent Material Systems and Structures*, vol. 6, no. 5, pp. 673–83, 1995.
- [14] G. P. Carman, "Nonlinear Constitutive Relations for Magnetostrictive Materials with Applications to 1-D Problems," in *Proceedings of the Second International Conference on Intelligent Materials. ICIM '94*, pp. 265–77, 1994.
- [15] S. Chikazumi, *Physics of Magnetism*. Robert E. Krieger Publishing Company, Inc., 1964.
- [16] J. D. Jackson, *Classical Electrodynamics*. John Wiley & Sons, 1962.
- [17] B. D. Popovic, *Introductory Engineering Electromagnetics*. Addison-Wesley Publishing Company, 1997.
- [18] I. M. Reed, R. D. Greenough, and A. G. I. Jenner, "Frequency-Dependence of the Piezomagnetic Strain Coefficient," *IEEE Transactions on Magnetics*, vol. 31, no. 6, pp. 4038–40, 1995.
- [19] D. A. Berlincourt, D. R. Curran, and H. Jaffe, *Piezoelectric and Piezomagnetic Materials and Their Function in Transducers*, pp. 169–270. *Physical Acoustics: Principles and Methods*, Academic Press, 1964.
- [20] R. M. Bozorth, *Ferromagnetism*. Van Nostrand, 1951.
- [21] F. Claeysen, N. Lhermet, R. LeLetty, and P. Bouchilloux, "Actuators, Transducers and Motors Based on Giant Magnetostrictive Materials," *Journal of Alloys and Compounds*, vol. 258, no. 1-2, pp. 61–73, 1997.
- [22] K. Prajapati, A. G. Jenner, M. P. Schulze, and R. D. Greenough, "Magnetoelastic Effects In Rare-Earth Iron-Aluminum Compounds," *Journal of Applied Physics*, vol. 73, no. 10, pp. 6171–3, 1993.
- [23] H. Wakiwaka, K. Aoki, T. Yoshikawa, H. Kamata, M. Igarashi, and H. Yamada, "Maximum Output of a Low Frequency Sound Source Using Giant Magnetostrictive Material," *Journal of Alloys and Compounds*, vol. 258, no. 1-2, pp. 87–92, 1997.

- [24] Q. Su, J. Morillo, Y. Wen, and M. Wuttig, "Young's Modulus of Amorphous Terfenol-D Thin Films," *Journal of Applied Physics*, vol. 80, no. 6, pp. 3604–6, 1996.
- [25] M. Wada, H. Uchida, and H. Kaneko, "Effect of the Substrate Temperature on the Microstructure and Magnetostrictive Characteristics of the $\text{Tb}_{0.3}\text{Dy}_{0.7}\text{Fe}_2$ Film," *Journal of Alloys and Compounds*, vol. 258, no. 1-2, pp. 143–8, 1997.
- [26] H. Q. Zhu, J. G. Liu, X. R. Wang, Y. H. Xing, and H. P. Zhang, "Applications of Terfenol-D in China," *Journal of Alloys and Compounds*, vol. 258, no. 1-2, pp. 49–52, 1997.
- [27] Etrema Products Inc., "Terfenol-D General Specifications," Product Specification, 1999.
- [28] T. S. Chin, F. M. Chen, and J. S. Fang, "Magnetostrictive Properties of $\text{Tb}_{0.3}\text{Dy}_{0.7}(\text{Fe}_{1-x}\text{V}_x)_2$ Alloys," *IEEE Transactions on Magnetics*, vol. 33, no. 5, pp. 3946–8, 1997.
- [29] L. Sandlund, M. Fahlander, T. Cedell, A. E. Clark, J. B. Restorff, and M. Wun-Fogle, "Magnetostriction, Elastic Moduli, and Coupling Factors of Composite Terfenol-D," *Journal of Applied Physics*, vol. 75, no. 10, pt.2A, pp. 5656–8, 1994.
- [30] D. Kendall and A. R. Piercy, "Comparison of the Dynamic Magnetomechanical Properties of $\text{Tb}_{0.27}\text{Dy}_{0.73}\text{Fe}_2$ and $\text{Tb}_{0.30}\text{Dy}_{0.70}\text{Fe}_2$," *Journal of Applied Physics*, vol. 76, no. 10, pp. 7148–50, 1994.
- [31] K. Prajapati, A. G. Jenner, and R. D. Greenough, "Magnetoelastic Behavior of Aluminum Substituted Terfenol-D At Elevated-Temperatures," *IEEE Transactions on Magnetics*, vol. 31, no. 6, pp. 3976–8, 1995.
- [32] S. C. Busbridge and A. R. Piercy, "Magnetomechanical Properties and Anisotropy Compensation In Quaternary Rare Earth-Iron Materials of the Type $\text{Tb}_x\text{Dy}_y\text{Ho}_z\text{Fe}_2$," *IEEE Transactions on Magnetics*, vol. 31, no. 6, pp. 4044–6, 1995.
- [33] K. Prajapati, R. D. Greenough, and A. G. Jenner, "Device Oriented Magnetoelastic Properties of $\text{Tb}_x\text{Dy}_{1-x}\text{Fe}_{1.95}$ ($x=0.27, 0.3$) At Elevated-Temperatures," *Journal of Applied Physics*, vol. 76, no. 10, pp. 7154–6, 1994.
- [34] N. Galloway, R. D. Greenough, A. G. I. Jenner, and M. P. Schulze, "Pressure Dependencies of Magnetostrictive Strain and D- Coefficient In Terfenol-D After Thermal or Magnetic Annealing," *Journal of Applied Physics*, vol. 76, no. 10, pp. 7163–5, 1994.

- [35] Dr. Antonios Giannakopoulos, 1999. Personal Communication.
- [36] J. Alcala, A. Giannakopoulos, and S. Suresh, "Continuous Measurements of Load-Penetration Curves with Spherical Microindenters and the Estimation of Mechanical Properties," *Journal of Materials Research*, vol. 13, no. 5, pp. 1390-400, 1998.
- [37] D. B. Montgomery, *Solenoid Magnet Design: The Magnetic and Mechanical Aspects of Resistive and Superconducting Systems*. Wiley-Interscience, 1969.